NASA TN D-3234

THERMAL RADIATION ABSORPTANCE AND VACUUM OUTGASSING CHARACTERISTICS OF SEVERAL METALLIC AND COATED SURFACES

By Takuo Mimura, Evelyn Anagnostou, and Paul E. Colarusso

Lewis Research Center
Cleveland, Ohio

NATIONAL AERONAUTICS AND SPACE ADMINISTRATION

For sale by the Clearinghouse for Federal Scientific and Technical Information
Springfield, Virginia 22151 – Price $3.00

THERMAL RADIATION ABSORPTANCE AND VACUUM OUTGASSING CHARACTERISTICS OF SEVERAL METALLIC AND COATED SURFACES

by Takuo Mimura, Evelyn Anagnostou, and Paul E. Colarusso

Lewis Research Center

SUMMARY

15791

Space simulating vacuum chambers frequently require walls of high thermal radiation absorptance. A number of surface coatings have essentially thermal blackbody absorptance characteristics; however, their utility may be limited by the requirement for maintaining high vacuum levels in the chamber. This report presents data on the thermal radiation absorptance and the vacuum outgassing characteristics of several commercial surface coatings that can be easily applied to chamber walls.

Sixteen stainless-steel specimens coated with organic paints, lacquer, and nylon were tested for normal spectral absorptance using a heated-cavity reflectometer (hohlraum) in conjunction with a double beam spectrophotometer over the wavelength range from 2 to 15 microns. Total normal absorptances for 1115° and 1500° F source temperatures were calculated from the experimental spectral data. Four of the higher absorptance coatings are missile black, black lacquer, Rust-Oleum silver gray, and Rust-Oleum white.

The outgassing tests were conducted by using a laboratory vacuum system apparatus with glass bell jar. The rate of outgassing was determined to permit a comparative evaluation between 29 metallic and painted metallic cylinders. Unpainted stainless-steel, aluminum, and copper specimens demonstrated the lowest outgassing rate, whereas nylon coated specimens showed the highest rate. Painted specimens showed more than 10 times as high an outgassing rate as that of the unpainted metal surfaces. The outgassing rate decreased when painted surfaces were previously baked or outgassed.

Also included in the report are the thermal radiation absorptance characteristics of oxidized AISI 316 stainless steel. Thirty six specimens with varying degrees of oxidization were tested. Some erratic results were observed when specimens were oxidized at 1400° and 1600° F; however, specimens oxidized at 1800° F consistently showed low spectral reflectance values that were relatively constant in magnitude, indicating a near gray-body characteristic.

author

INTRODUCTION

Research and development activities connected with space vehicle components frequently require testing and evaluation in a simulated space environment. Generally, space simulation requires high absorption of thermal energy and high vacuum. Pressures in space vary from 10^{-3} torr in near space to 10^{-16} torr or lower in interplanetary space. The predominant mode of heat transfer in space, therefore, is thermal radiation. In order to minimize gas conduction effects, when heat-transfer tests are conducted, vacuum levels of 10^{-4} to 10^{-5} torr are generally maintained in the space simulating chamber (ref. 1). At this pressure level, the simulator walls will start releasing gases from their surfaces. The amount of the gases thus released will depend on the vacuum level inside the simulator as well as the surface conditions of the chamber walls. The walls of space simulating vacuum chambers, therefore, must possess high absorptance for incident thermal energy and at the same time should be able to maintain the required high vacuum level. The desired absorptance characteristics are generally obtained by the application of surface coatings to metallic vacuum chamber walls.

Special and commercial paints are frequently used as coatings. These paints possess favorable absorptance characteristics, are easily applied to a large complex surface, are inexpensive, and are readily obtained. On the other hand, the painted surfaces are limited in operating temperature range, are chemically and physically less stable than metallic surfaces, and often make high vacuum levels difficult to attain because of their usually high outgassing rates. (Outgassing rate is indicative of the amount of gas released from a unit surface in a vacuum per unit time.) An ideal coating for the simulating chambers, therefore, is the one which has the combination of high absorptance characteristics and low outgassing rate.

The data on the absorptance of paints that are available to date are limited and are mostly for the visible spectrum range (0.4 to 0.7 μ), while information on the thermal spectrum range (1.0 to 100 μ) are necessary for application to the simulating chamber walls for tests involving heated components. Some outgassing data on metals and plastic has been published, but they are difficult to correlate and compare with each other because of the difference in measuring techniques, time of outgassing, ratio of pumping speed to specimen dimensions, ionization gage errors, and other variables (ref. 2). The data on the outgassing rates of paints are virtually unavailable.

The purpose of this report is twofold. First, to present data on the thermal absorptance characteristics of several coatings with emphasis on commercial paints. Second, to present comparative data on the outgassing rates of several painted and unpainted metal specimens.

The report is supplemented by the data on thermal radiation absorptance of AISI 316 stainless steel with various degrees of oxidation. The experiment on the oxidized stain-

less steel was conducted primarily to determine a suitable coating for a high temperature radiant condenser application. The data on stainless steel are included for general interest rather than for specific application to simulating chambers.

The report consists of two major sections. The first section deals with infrared radiation absorptance characteristics of coated and oxidized surfaces. The second section will discuss the outgassing rates of coated and uncoated metallic surfaces. Each section consists of subsections covering the theory, test apparatus, specimens, accuracy of measurements, and results.

THERMAL RADIATION ABSORPTANCE

The thermal radiation absorptance of space simulating chamber walls becomes a prime consideration when the chamber is designed for thermal testing. In order to simulate closely the space environment, the reflection of thermal energy from the wall must be minimized. Space power generating systems under current study (ref. 3) have waste-heat radiators operating at temperatures of 500° (Brayton cycle) to 1400° F (Rankine cycle). For thermal testing of the components of the systems the chamber walls should possess a high absorptance of thermal energy. Uncoated surfaces of most metals typically have spectral absorptance values ranging from 0.1 to 0.4. Consequently, coatings are generally applied to metallic surfaces to improve their absorptance characteristics. Experiments were conducted to obtain spectral absorptance data on various commercially available surface coatings that appeared promising for application to the chamber walls.

An outline of the theory underlying the measurement procedures and the data reduction procedures for computing the total hemispherical absorptance and the total normal absorptance of a sample from the spectral normal reflectance data is presented in appendix A. A brief discussion of the variation of absorptance with the sample temperature and the source temperature is also included in the appendix.

Test Apparatus

The spectral absorptance of opaque surfaces may be determined either by measuring spectral reflectances or by measuring spectral emittances. In the current investigation, spectral reflectances were measured. The spectral reflectance measurements are preferable to spectral emittance measurements for most purposes because of the following (ref. 4):

(1) Reflectance measurements provide accurate values over a much wider spectral range than do emittance measurements (because energy is supplied from an external

source rather than emitted from the sample).

(2) Reflectance measurements do not require precise knowledge of sample temperatures, which is a critical factor in emittance measurements.

(3) Reflectance measurements can tolerate a large variation in sample temperature with a small error in the spectral reflectance.

There are two basic methods in spectral reflectance measurements. In the first method, the sample is diffusely irradiated in a blackbody cavity, and the intensity of the reflected radiation is measured in an angle normal to the specimen surface. In the second method the sample is irradiated by a narrow beam at an angle of incidence, and the reflected energy is collected either by an integrating sphere or a suitable mirror system. This method, however, is generally limited to the short wavelength range (to 2.5μ) (ref. 5). In the current investigation the first method was employed. The test apparatus used commercial equipment capable of measuring normal spectral reflectance of infrared radiation over the wavelength range of approximately 2 to 15 microns.

A general schematic view of the measuring apparatus is shown in figure 1. The basic system consists of spectrophotometer, hohlraum, optical transmitters, and temperature controllers. Detailed descriptions of the construction and operation of the apparatus is given in reference 6; therefore, only a brief summary is presented herein.

Figure 2 shows a detail of the hohlraum used in the experiment. It is a heated cavity with isothermal walls providing the radiation source for both sample and reference beams and is constructed to possess blackbody emittance characteristics of at least 0.98. The hohlraum cavity is contained in a double stainless-steel radiation shield. The cavity wall is made of nickel and is heated electrically to maintain its temperature at $1112^{\circ}\pm18^{\circ}$ F.

A sample mounted in the sample holder (fig. 2) will be irradiated diffusely by the hohlraum wall. Some of the energy reflected passes through a small hole in the bottom of the hohlraum and is transmitted by suitable transfer optics (fig. 1) to a spectrophotometer. A portion of the wall is viewed alternately with the sample, and the intensity of its radiation is compared with that reflected from the sample for optical analysis by the spectrophotometer. The sample holder is water cooled. A water regulator maintains the sample temperature at $80^{\circ}\pm5^{\circ}$ F, which is approximately that of the temperature of the spectrophotometer detector. For wavelengths of 15 microns and less, sample temperature variation of $\pm5^{\circ}$ F produces a negligible effect on the reflectance readings, as described later in the section, Accuracy of Measurement.

The transfer optics directing the beams originating from the reference and sample areas into the spectrophotometer consists of a series of plane and spherical mirrors. The effects of atmospheric absorptance were nullified by making the sample- and reference-beam path lengths equal and the number of reflections in each path the same. Suitable enclosing baffles were installed as a precaution against convective currents in the ambient atmosphere.

Specimens

Each sample disc on which the coatings were applied was machined from AISI 316 stainless-steel bars to a diameter of 0.94 inch and a thickness of 0.05 inch. Surfaces were finished to 32 root mean square. Stainless steel was used because vacuum chamber walls are generally constructed from stainless steel. The coating specimens selected were commercially available oil-base paints, lacquers, and plastics that appeared suitable for application to the chamber walls because of their chemical stability, adhesion, resistance to wear, and ease of application. A total of 16 coated specimens were prepared as listed in table I(a). The coatings were applied to the specimens by spraying to an average thickness of 1.5 mils and dried in air for a minimum of 24 hours. The specimens of the oxidized stainless steel were of the same size and material as used for the coated specimens. The specimens were grit blasted before they were oxidized to insure adherance of the oxide films and also to improve their absorptance characteristics. The oxidation was carried out by heating the specimens in air in an electric furnace at different temperatures for varying lengths of time. Details of the oxidized specimen characteristics are given in table I(b).

Experimental Procedure

Operation of the hohlraum and the spectrophotometer is described in detail in reference 6. Only a brief description therefore is given herein. The spectrophotometer is a double-beam type, which scans the two beams alternately and records the ratio of the radiant intensities of the two beams. A continuous spectrum of spectral normal reflectance throughout the scanning range from 2 to 15 microns is obtained.

The hohlraum must be adjusted before each series of tests is made. The adjustment consists in setting a 100-percent level and a zero-percent level in the spectrometer reading. The 100-percent level is obtained by comparing two beams originating at the hohlraum top wall when the hohlraum is rotated 90° from the sample position. After the 100-percent level has been established, the hohlraum is returned to the sample position. The zero-percent level is then obtained by blocking the sample beam and by comparing the reading of the blocked beam with that of a reference beam from the hohlraum top wall. The sample reading, which is the ratio of the radiant intensity of the sample to that of the reference beam, is recorded between the zero- and 100-percent levels. The three ratios measured and recorded in determining the normal spectral reflectance of a sample are as follows:

$$r_{100} = \text{100-percent level} = \frac{J_2'}{J_2''}$$

$$r_o = \text{zero-percent level} = \frac{J_o}{J_2}$$

$$r_s = \text{sample level} = \frac{J_s}{J_2}$$

where

J_2' spectral radiance of hohlraum top wall viewed by one beam

J_2'' radiance of same wall viewed by other beam when the hohlraum is rotated 90^o from sample position

J_o zero-level intensity obtained by blocking sample beam, closely approximates blackbody radiance at room temperature

J_2 spectral radiance of reference beam originating from hohlraum top wall when hohlraum is in sample position

The normal spectral reflectance is computed by

$$\rho_{\lambda,N} = \frac{r_s - r_o}{r_{100} - r_o} = \frac{\frac{J_s}{J_2} - \frac{J_o}{J_2}}{\frac{J_2'}{J_2''} - \frac{J_o}{J_2}} \tag{1}$$

Assuming a uniform wall temperature, that is, $J_2' = J_2'' = J_2$, yields

$$\rho_{\lambda,N} = \frac{J_s - J_o}{J_2 - J_o} \tag{2}$$

A typical hohlraum chart recording is shown in figure 3. The wavelengths are determined by counting the number of revolutions of a wavelength-drive drum. A maximum of 150 points is possible, but 25 points, which are considered adequate to define the curve

without loss of accuracy, were used in the current test.

The individual samples were mounted on the sample holder located in the top wall of the hohlraum (fig. 2). The samples were oriented at an angle approximately perpendicular to the optical path of the final mirror in the sample beam of the transfer optics (see fig. 1). Measurements taken on the samples in this position, therefore, yield the spectral near-normal reflectance of the sample.

Accuracy of Reflectance Measurement

A detailed analysis of the uncertainties and errors associated with the reflectance measurement by using the hohlraum in conjunction with the double beam spectrophotometer has been performed by Streed, et al. (ref. 7). The three major sources of errors are nonisothermal hohlraum wall temperature, sample temperature variation, and errors connected with transfer optics and spectrophotometer.

According to the experiments conducted in reference 7, the first error is the largest for high-reflectance materials and the least for low-reflectance materials such as black paints. Theoretically, the errors caused by nonuniform-cavity wall temperature should be higher at short wavelengths and should increase with the temperature level of the wall. In reference 7, the error was calculated to be less than ±0.01 reflectance unit for an oxidized stainless-steel specimen for wall-temperature variations of $1488^{\circ} \pm 52^{\circ}$ F at the top, $1582^{\circ} \pm 50^{\circ}$ F at the side, and $1465^{\circ} \pm 126^{\circ}$ F at the bottom.

In the experiment conducted herein, hohlraum temperature variations were maintained within $\pm 18^{\circ}$ F from the mean temperature of 1112° F at the top, side, and bottom, and the error from the nonuniform wall temperature should therefore be less than ±0.01 reflectance unit.

The second error caused by variation in sample temperature was minimized by setting the cooling-water temperature of the sample holder at $80^{\circ} \pm 5^{\circ}$ F. An experiment in reference 6 indicated that the reflectance reading varied by 0.01 reflectance unit at a wavelength of 16 microns for black paint with a sample temperature variation of 27° F and by 0.02 reflectance unit for oxidized stainless steel with a sample temperature variation of 54° F. At a wavelength of 6.1 microns the errors dropped to 0.001 and 0.002 reflectance unit for black paint and oxidized stainless steel, respectively, for the same temperature variations. The temperature variation in the current test is much less than that used in the above experiment; consequently, the error due to the sample temperature variation will be negligible.

The error in the optics and photometer was assessed by comparing the repeated measurements of a sample. Observations of such a comparison indicated the results were reproducible within ±0.01 reflectance unit.

Based on the preceding discussion the overall error of the spectral reflectance mea-

surement for this experiment is estimated to be less than ±0.02 reflectance unit.

Results and Discussions of Thermal Radiation Absorptance Measurement

Coated surfaces. - Figures 4(a) to (p) show the spectral normal reflectance as a function of wavelength for the 16 coated samples tested (table I(a)). In general, the painted surfaces have a smaller value of reflectance at the longer wavelengths than they have at the shorter wavelengths. An exception to this general trend is indicated by the clear coatings (no pigments) of specimens 5 and 15, which showed large reflectance values at the longer wavelengths. These observed characteristics can be explained from a general understanding of the mechanics of reflectance of surface coatings.

If a metal is coated with a film of paint, reflections will occur at each interface between the pigment particles and the binder of the paint. This is characteristic of a diffusing medium consisting of a large number of small particles of given optical properties distributed in a second medium of different optical properties. If the coat of paint is sufficiently thick, very little incident radiation will reach the base metal because of multiple interreflections within the paint film. Reflectance characteristics then become almost completely dependent on the optical characteristics of the pigment and binder combination.

On the other hand, if a surface coating is transparent, the reflectance will be determined by a combined effect of the refraction index and absorption coefficient of the film and the surface characteristics of the substrate, particularly the surface roughness.

Pigments and binders of most commercial paints are oxides and resins that are electrical nonconductors. A characteristic feature of nonconductors is their generally lower reflectance values at longer wavelengths; however, this relation does not hold for the visible or shorter wavelength range (ref. 8). This can be seen by comparing the black coating (figs. 4(a) and (b)) with the white coating (figs. 4(c) and (d)). Both the white and the black specimens have relatively low reflectance at longer wavelengths. The white coatings, however, show increasingly higher reflectances toward the shorter wavelengths while the reflectance of the black coating tends to decrease with wavelength.

The group of Rust-Oleum paints shown in figures 4(e) to (i) have similar reflectance patterns. Although magnitude of the reflectance at each wavelength varies, all of the paints have a major absorption band between wavelengths of 3 and 4 microns. Rust-Oleum clear in figure 4(e) shows somewhat higher and irregular reflectances at the longer wavelengths because of the combined effect of the absorption of the paint and the reflectance of the stainless-steel substrate. The substrate reflectance usually increases with wavelength.

Figures 4(d) and (k) show reflectances for white lacquer and zinc chromate coated specimens. Figures 4(m) and (n) are for the same specimens with an additional coating

of nylon. The specimens with an additional nylon coating have slightly lower reflectance values compared with the specimens without nylon coating. Although the nylon film appears transparent in the visible wavelength region, it is apparently opaque and absorbs some of the infrared radiation. Figure 4(o) represents a specimen that was first vapor blasted and then coated with nylon. The higher and irregular reflectances at longer wavelengths are believed to have been caused by the strong absorption bands in the nylon combined with reflection from the metallic base. Irregular and multiple absorption bands in the nylon are typical of an organic plastic composed of strings or chains of molecular groups (ref. 9).

The total normal absorptances calculated from the spectral normal reflectances of figure 4 by graphical integration of equation (A16) in appendix A are tabulated in table II for temperatures of 1112° and 1500° F. The calculation was performed over the wavelength range from 2 to 15 microns. Total blackbody radiation intensity was calculated by using data in reference 8. Both the missile black and black lacquer coated specimens (specimens 1 and 3) have the highest values of all tested and the nylon coated sample (specimen 15) has the lowest value for the wavelength range considered in this experiment. As previously mentioned, all the data were obtained at a sample temperature of approximately 80° F and a source temperature of 1112° F.

Oxidized surfaces. - Figures 5(a) to (e) show the spectral normal reflectances of AISI 316 stainless steel oxidized at 1200° F for the individual oxidization time and substrate roughness listed in table I(b). Figures 5(f) to (i) show data on samples oxidized at 1800° F for the same parameters. The reflectance of oxidized 316 stainless steel is generally higher than that of the painted surfaces.

Observation of the first set of data (figs. 5(a) to (e)) indicates that the reflectances increased fairly rapidly with wavelength for the samples oxidized for 1, 4, and 8 hours; however, the rate of increase was reduced for the samples oxidized for 16 and 24 hours.

Also, increasing roughness of a surface tends to make the surface diffuse, and the reflectance curve tends to become flat over the entire wavelength range.

Reference to figures 5(f) to (i) for samples oxidized at 1800° F shows that the oxidation process proceeded more rapidly and as a result, oxidation for 2 and 6 hours and longer did not produce a great difference in the reflectance measurements. Furthermore, it was observed that the oxidized surface possessed nearly gray-body characteristics with relatively low and constant reflectance values throughout the wavelength range and that surface roughness had little effect on the reflectance value.

The data obtained for the samples oxidized at 1400° and 1600° F are rather erratic, and it is difficult to draw a general conclusion. The erratic result was apparently caused by the imperfect mechanical bonding between oxides and metal. During the preparation of the specimen it was observed that portions of the oxide film were removed by cracking and scaling at temperatures of 1400° and 1600° F.

The data for 1400° and 1600° F are presented in tables III(a) and (b).

Total normal absorptances of stainless-steel samples oxidized at 1800° F for 2, 6, 16, and 24 hours were calculated for incident radiation of two temperatures in the same manner as that used for the painted samples and are tabulated in table IV. There are some inconsistencies in the calculated values; for instance, a sample oxidized for 2 hours has a total absorptance value of 0.86 as compared with 0.82 for the sample oxidized for 6 hours. Similarly, a sample oxidized for 16 hours has an absorptance value of 0.88 as compared with 0.84 for a sample oxidized for 24 hours. The samples oxidized for longer periods should have higher absorptances. These inconsistencies apparently resulted from imperfect bonding between oxide film and metal substrate as mentioned previously. These observations of the experimental results indicate the difficulties encountered in obtaining an oxidized surface with uniform and consistent absorptance characteristics.

OUTGASSING RATE

This portion of the report will present the results of the outgassing measurements on coated and uncoated metals together with theory and pertinent comparisons. The data are intended for a comparative evaluation of the surfaces and for use in the general specification of surface coatings for the walls of space-simulating vacuum chambers. In the experiment the vacuum level ranged from 1×10^{-3} to about 4×10^{-6} torr, which defines the area of application of the results.

Theory

Outgassing rate K. - The amount of outgassing is preferably expressed by the outgassing rate K, which is expressed in units of (torr)(liters)/(sec)(cm^2) at a specified temperature (ref. 2). The outgassing rate K thus defined indicates the amount of gases evolved from a unit surface area per unit time at a specified pressure and temperature. The outgassing rate is an instantaneous value since the outgassing rate is a function of system pressure that changes continuously as outgassing proceeds.

The relation between pressure and outgassing rate for a specimen in a bell jar is derived from the principle of material balance (ref. 2):

$$SP = K_S A_S - L_S A_S - V_B \frac{dP}{dt} + K_B \tag{3}$$

where S is a net pumping speed at a place where pressure P is measured and is

related to pump speed S_p by

$$\frac{1}{S} = \frac{1}{S_p} + \frac{1}{U} \tag{4}$$

where

S net pumping speed, liter/sec

S_p pump speed, liter/sec

P total pressure in the vacuum chamber at any instant, torr

U conductance (reciprocal of flow-resistance) between pump and vacuum chamber, liter/sec

K_s free outgassing rate of the specimen, (torr)(liter)/(sec)(cm^2)

A_s specimen surface area, cm^2

L_s free sorption rate of the specimen, (torr)(liter)/(sec)(cm^2)

V_B displacement of the bell jar, liter

t time, sec

K_B total outgassing load of empty bell jar, (torr)(liter)/sec

The total outgassing load of the empty bell jar K_B includes the air leak through joints of the vacuum system, the gases that permeate through the bell jar wall and the gasket, and the oil migration from the diffusion pump through the baffle and cold trap (see fig. 6). The difference between the free outgassing rate and the free sorption rate $K_s - L_s$ is the net amount of evolved gas and is defined as the outgassing rate, K. During the measurement the jar is sealed off from the pumping system; hence $S = 0$. Therefore, equation (3) reduces to

$$K_s - L_s = K = \frac{V_B}{A_s}\frac{dP}{dt} - \frac{K_B}{A_s} \tag{5}$$

where dP/dt is measured for the particular specimen for which A_s is known and K_B, a characteristic of the particular bell jar system, is determined for the empty bell jar volume V_B. With the specimen removed from the bell jar, equation (3) becomes

$$K_B = V_B \frac{dP}{dt} \tag{6}$$

In the following experiments an average pressure rise rate $\Delta P/\Delta t$ was measured over a given pressure range instead of an instantaneous value dP/dt.

Relation between system pressure and pump speed. - To calculate the system pressure P at any time t for a given pump speed S and a given system volume V_B, equation (3) may be integrated by using average values of K and K_B over the pressure range of integration and setting $L_s = 0$, since free sorption is negligibly small during pumpdown (ref. 2).

$$P = P_o e^{-\frac{St}{V_B}} + \left(1 - e^{-\frac{St}{V_B}}\right) \frac{K_s A_s + K_B}{S} \tag{7}$$

The ultimate pressure P_u is obtained when t approaches ∞. From equation (7) by setting $T = \infty$

$$P_u = \frac{K_s A_s + K_B}{S} \tag{8}$$

The ultimate pressure depends on the pump speed S for a given vacuum system. When the ultimate pressure is attained, the pump speed will be in equilibrium with the outgassing rate from the exposed surface of the materials inside the vacuum chamber and the permeation and leaks through the chamber walls and joints of the vacuum system.

Relation between free outgassing rate K_s, free sorption rate L_s, and outgassing rate K. - As previously mentioned (in the section, Outgassing rate K), the outgassing rate K is the difference between the free outgassing rate K_s and the free sorption rate L_s and may be calculated from the rate of average pressure rise $\Delta P/\Delta t$. It is difficult, however, to determine experimentally individual values of K_s and J_s. If the outgassing rate K of a specimen is small, it may generally be assumed that the outgassing rate K is approximately equal to K_s, since the free sorption rate J_s is small for most of the common material (ref. 10). A required pump speed for a vacuum system may then be estimated by using equation (8) and setting $K_s = K$

$$S = \frac{KA_s + K_B}{P_u} \tag{9}$$

where values of K and K_B are obtained experimentally.

Test Apparatus

The bell jar system used in this experiment is composed of commercially obtained laboratory vacuum components, slightly modified at the Lewis Research Center. A schematic drawing showing two views of the equipment is shown in figure 7. It consists of a support table, a glass bell jar, an evacuation system, and necessary instrumentation. The slight modifications included the alteration of a disk-type vacuum valve so that the valve disk rotates 90° when it is fully opened to minimize the impedance to the flow and the insertion of a stainless-steel spool piece between the bell jar table and the diffusion pump for mounting a thermocouple gage and an ion gage. The evacuation system is a High Vacuum Equipment Corporation (HVEC) modified CP6-15 system consisting of a mechanical roughing pump, a mechanical holding pump, and a 6-inch cold-trapped oil diffusion pump. Instrumentation to record the pressure in the bell jar includes a hot filament ionization gage (HVEC Type G-71-4) and a thermocouple gage (HVEC Type G-72). The thermocouple gage was used to measure the pressure down to 10^{-3} torr and the ionization gage from 10^{-3} torr down to approximately 10^{-6} torr. The various pump capacities are as follows:

(1) Mechanical roughing pump: 15 cu ft/m at 14.7 psia, 60° F

(2) Mechanical holding pump: 2 cu ft/m at 14.7 psia, 60° F

(3) Oil diffusion pump: 900 liters/sec at 10^{-6} torr

The volume of the bell jar is 135 liters. The empty bell jar system is capable of maintaining approximately 10^{-5} torr vacuum without a liquid nitrogen cold trap and 10^{-6} torr with a cold trap.

Test Specimens

The cylindrical test specimens were prepared in two sizes, 18-inch outside diameter by 16-inch length and 14-inch outside diameter by 12-inch length, both with a wall thickness of 3/8 inch. Painted specimens were fabricated from ASTM A53 low-carbon-content steel pipe. Stainless-steel, aluminum, and copper specimens without surface coatings were made of 3/8-inch-thick plate rolled into cylinders.

A total of 29 specimens were prepared. Paints were applied to both sides of the cylinders either by brush or spray to a thickness specified in the manufacturer's recommendations. The coatings, which were tested previously for radiation absorptance measurements, are as follows: missile black, Rust-Oleum clear, Rust-Oleum red, Rust-Oleum white, zinc chromate, white porcelain, white lacquer, and nylon. Film thickness specified for these specimens was the same as that used in the absorptance measurements. All the samples were sandblasted with grit 80 abrasive and were vapor degreased

prior to the application of the coatings. The vapor degreasing was carried out by exposing the specimens to trichlorethylene vapor heated to about 180° F. A detailed description of the treatment of the individual specimens is given in table V.

Experimental Procedure

The evacuation process of the bell jar was performed in two steps. First, by using the mechanical roughing pump (fig. 7), the bell jar was pumped down to approximately 5×10^{-3} torr. Then the diffusion pump in series with the holding pump was started and continued to operate until a pressure of approximately 4×10^{-6} torr was attained. When the 4×10^{-6} torr was reached, a vacuum valve was closed to seal off the bell jar from the pumping system, which left the specimen in the bell jar to outgas freely. The change of pressure was recorded as a function of time during this period. When the pressure reached a level of 1×10^{-3} torr, the vacuum valve of the diffusion pump was reopened, and the second pumpdown cycle was started. The same procedure used for the first pumpdown was repeated in the second cycle. For most of the specimens, two pumpdown cycles were performed.

Accuracy of Outgassing Measurement

The major sources of uncertainties associated with the outgassing measurements may be classified into three groups:

(1) Reliability of the ionization gage

(2) Variation of atmospheric conditions during the tests

(3) Lack of exact specifications of the surface characteristics of the test specimens

The particular ionization gage used in this investigation was a conventional hot-filament triode ionization gage, which is generally accepted as adequate to measure a vacuum to 10^{-8} torr. It was calibrated by a McLeod gage for nitrogen gas with an accuracy of ±1 percent down to about 10^{-4} torr. The calibration at pressures below 10^{-4} torr was obtained by extrapolation. The estimated accuracy of the vacuum reading with the ionization gage calibrated in this manner is ±10 percent at 10^{-6} torr.

The accuracy of pressure measurement with the ionization gage, however, depends on the composition of the gas present. If a gage calibrated for nitrogen is used for gases other than nitrogen, its pressure reading will not be correct any longer. The available data on the calibration of ionization gages for several single gases show that a gage calibrated for nitrogen may read one-sixth of actual pressure for helium and one-half of actual pressure for hydrogen (ref. 10). Therefore, without a knowledge of the specific

composition of gases in the vacuum system, the error in pressure reading cannot be predicted.

The second source of uncertainty is the variation of atmospheric conditions during the outgassing tests. The vacuum level in the bell jar was sensitive to variations in ambient temperature. For instance, when the temperature was recorded with a mercury thermometer attached to the bell jar, the vacuum in the empty bell jar fell from 9.6×10^{-6} torr at 85° F to 7.1×10^{-6} torr at 75° F and to 4.6×10^{-6} torr at 65° F. The pressure was recovered to the original level when the temperature was restored. With the specimen placed inside the bell jar, a similar variation of pressure with temperature should occur. The room temperature throughout the tests varied between 85° and 70° F, and the pressure reading error due to this variation is estimated to be ±15 percent.

Variation of humidity and barometric pressure will also have some effect on the initial pumpdown speed; however, once the bell jar pressure reaches the 10^{-4} torr level, it is believed that pumpdown speed depends entirely on the outgassing rates of the exposed surfaces and external leaks. The external leaks were compensated for, as previously described (in the section, Outgassing rate K), in the calculation of the outgassing rates.

The third source of error is the most serious one and is the main reason that makes the achievement of accurate and reproducible experiments on outgassing extremely difficult. Local variations of sorption characteristics frequently produce different results between two samples of the same material. Even an identical sample may outgas more or less depending on its vacuum history and the length of time of exposure to atmosphere. Random errors are introduced by nonuniform surface roughness, existence of dirt and water vapor on surfaces, and microscopic voids in paint and oxide films.

The preceding discussion undoubtedly restricts the reliability and the usefulness of the data for exact calculations. Nevertheless, it is felt that data should provide enough information to meet the immediate need of making engineering estimates and comparisons of the behavior of vacuum chamber walls.

Results and Discussions of Outgassing Measurement

The results of the experiments are presented in figures 8(a) to (q), where pressure and time are plotted on log-log scales for the pumpdown and outgassing cycles. As previously mentioned, the K values were calculated based on the average pressure rise rate $\Delta P/\Delta t$. Consequently, the K values thus obtained will result in the average values for a specified pressure range ΔP. However, since the outgassing curves of most of the samples demonstrated straight lines at an approximately 45° angle with the abscissa on log-log scales, the $\Delta P/\Delta t$ is very nearly equal to dP/dt.

From the fact that the pressure and time relation during outgassing can be repre-

sented by a straight line on log-log scales, a functional relation between P and t exists in the form of $P = at^b$ where a and b may be called outgassing indexes, denoting the initial pressure and the slope of the straight line, respectively. The initial pressure was arbitrarily set at the pressure 1 minute after the vacuum valve was closed to seal off the bell jar from the pumping system. Comparison of the values of the indexes, a and b, yields evaluations of the outgassing characteristics of different specimens.

The outgassing rate K (eq. (5)) and the outgassing indexes a and b calculated in this manner are tabulated in table VI.

The results should not be construed as representing absolute values but rather should be regarded as providing a basis for a qualitative and comparative evaluation of the outgassing characteristics of different coatings.

Empty bell jar. - Figure 8(a) shows a typical pressure-time history of the empty bell jar. The pumpdown time for atmospheric pressure to approximately 4×10^{-6} torr took about 26 minutes. When the vacuum valve was closed to seal off the pumping system, the pressure rose abruptly to about 3.6×10^{-5} torr in less than 1 minute. This abrupt increase of pressure, or pressure burst, is apparently caused by trapped gas in the valving mechanism and gas leaks through seals during the valve operation. The magnitude of the pressure burst depends on the particular valve design and the gas present in the bell jar. The curve in figure 9(a) shows that the pressure burst for the first, second, and third pumpdowns was approximately of the order of 1 decade (from 1.8×10^{-6} to 2×10^{-5} torr for the second pumpdown, and from 1.4×10^{-6} to 1.4×10^{-5} torr for the third pumpdown). The pressure burst was greater when outgassing samples were present in the bell jar, as is shown in figures 8(d) to (q).

Metallic surfaces. - Figures 8(b) and (c) show results for severely and slightly rusted carbon steel samples, respectively. The pumpdown and outgassing curves indicate a lengthy time requirement for both outgassing and pumpdown. In table IV, it is seen that the time from vacuum valve closing to 10^{-3} torr is extremely long compared with that of the empty bell jar. The calculated K values are negative, indicating that the pressure rise rate during the outgassing process was less than that of the empty bell jar. This implies that the rusted carbon steel surface sorbed more gases and vapors than were outgassed during the free outgassing process. Referring to equation (3), since K is negative, shows that the free sorption rate L_s is larger than the free outgassing rate K_s. This peculiar behavior of the rusted steel samples could be explained by the fact that the rusted steel samples have irregular and porous surfaces, providing a large area for trapping and absorbing the exterior gases and vapors.

Figures 8(d) and (e) show pumpdown and outgassing curves for sandblasted carbon steel and for sandblasted and vapor-degreased carbon steel samples. Pumping time required from atmospheric pressure to 4×10^{-6} torr is 98 minutes for the first sample and 90 minutes for the second sample in contrast with 650 and 530 minutes for the two previous

rusted samples. The calculated K values, however, still show negative values, which indicates that the surface is sorbing the gases and vapors, although to a lesser degree than the rusted steel samples. Caution, therefore, has to be exercised in estimating pump speed using equation (9) for a system involving a carbon steel structure. Although the outgassing rate K appears small or even negative, the free outgassing rate K_s and the free sorption rate J_s are both large numbers as demonstrated by the long pumpdown-time requirements. Thus, assuming K equal to K_s in estimating pump speed for rusted carbon steel chambers will result in an erroneous answer.

Figures 8(f) and (g) represent the stainless-steel, aluminum, and copper samples. When compared with the carbon-steel samples, it is clearly noticeable that the pumpdown times for these metals are markedly shorter. Values of K for the first outgassing are 0.01×10^{-7}, 0.04×10^{-7}, and 0.05×10^{-7} (torr)(liter)/(sec)(cm^2) for stainless steel, aluminum, and copper, respectively, which indicate low outgassing and low sorption rates.

Coated surfaces. - Figures 8(h) through (q) represent the pumpdown and outgassing characteristics for various organic coatings. The shortest initial pumpdown time, 90 minutes, was recorded by Rust-Oleum clear (specimens 14, 15, and 16) in figure 8(k) and the longest, 1690 minutes, by Rust-Oleum white (specimen 23) in figure 8(n). The calculated outgassing rate K ranged from 0.23×10^{-7} (torr)(liter)/(sec)(cm^2) for baked Rust-Oleum clear (specimen 16) in figure 8(k) to 1.84×10^{-7} (torr)(liter)/(sec)(cm^2) for nylon (specimen 29) in figure 8(q).

The outgassing index a, which represents the initial pressure in outgassing, also indicates the magnitude of pressure burst previously mentioned (in the section, Empty bell jar). In general, index a was small for specimens with low K values and large for specimens with high K values. For the baked Rust-Oleum clear (specimen 16), which has the lowest K values, index a was 12×10^{-5}, and for the nylon (specimen 29), which has the highest K value, index a was 82×10^{-5}.

Phenoline (specimens 24 and 25) in figure 8(o) recorded an exceedingly lengthy pumpdown time and a very fast pressure recovery (50 and 23 sec for recovery to 10^{-3} torr for specimens 24 and 25, respectively). This indicates the high content of volatile elements in these samples. Values of K for phenoline samples were not calculated because of their obviously severe outgassing characteristics.

Table II shows that missile black (specimen 1), Rust-Oleum gray (specimen 5), and Nylon-coated white lacquer (specimen 11) possessed, in the order mentioned, the three highest total normal absorptances. Table VI, however, shows these coatings also have high outgassing rates of 1.03×10^{-7}, 1.15×10^{-7}, and 1.84×10^{-7} (torr)(liter)/(sec)(cm^2), respectively. The high outgassing rate is, of course, not desirable from the viewpoint of achieving a high vacuum. In selecting suitable coatings for a vacuum chamber, it is therefore necessary to consider whether the major emphasis of the simulation of the effects of space environment is in high vacuum or in high absorptance or both. Such con-

sideration is to be determined by the type of the experiments to be performed in the vacuum chamber.

In all the samples tested the second pumpdown time, as expected, was much shorter than the first. Also, the baked samples resulted in shorter pumpdown time and lower outgassing rate. Typical examples are Rust-Oleum clear (specimens 14, 15, and 16 in fig. 8(k)). Specimen 14 was dried in air for 24 hours, specimen 15 baked for 4 hours at 150° F, and specimen 16 baked and further exposed to dry air for 24 hours. The outgassing rates for these samples are 0.50×10^{-7}, 0.41×10^{-7}, and 0.23×10^{-7}(torr)(liter)/(sec)(cm^2), respectively. The same holds true, although to a lesser degree, for the following pairs of samples: samples 8 and 9 (thin Glyptol), 10 and 11 (thick Glyptol), 12 and 13 (missile black), and 20 and 21 (Rust-Oleum green on white). If paint coatings are to be used in vacuum service, it is therefore advisable to apply thin coats first and either vacuum outgas or bake between successive coatings.

SUMMARY OF RESULTS

Measurements of spectral normal reflectances of stainless-steel samples coated with paints, lacquers, and nylon indicated that, with the exception of nonpigmented clear coatings, they all exhibited the reflectance characteristics of electrical nonconductors; that is, the reflectance is generally low at longer wavelengths. Missile black and black lacquer both indicated the lowest reflectance values throughout the spectrum, whereas missile white and white lacquer exhibited increasingly high reflectance values at low wavelengths. Nonpigmented coatings such as nylon and Rust-Oleum clear demonstrated irregular and high reflectances at longer wavelength caused by strong absorption bands typical of organic plastics combined with reflection from the metallic substrate.

The total normal absorptances at two incident energy temperatures calculated from the spectral normal reflectance measurements showed that missile black, black lacquer, Rust-Oleum gray, and white coatings possessed the highest values (0.94 to 0.83) and the nylon-coated sample the lowest value (0.70).

Reflectances of oxidized AISI 316 stainless steel were in general not as low as the painted surfaces. It was observed that the samples oxidized at 1800° F showed the lowest reflectances (approx 0.2), which were fairly constant with wavelength. This observation indicates almost gray-body characteristics. Some erratic results were observed for the specimen oxidized at 1400° and 1600° F due to the loss of a portion of the oxide coatings. Observation of the experimental results of oxidized 316 stainless steel indicates that it is difficult to obtain an oxidized surface with uniform and consistent absorptance values.

Outgassing tests were conducted to achieve a comparative evaluation of the outgassing characteristics of various coatings and metals. Due to several uncertainties associated

with outgassing measurements, it was difficult to obtain repeatable results. From the outgassing tests, however, the following general results were derived:

1. Carbon steel, especially rusted carbon steel, apparently sorbs gases and vapors at a faster rate than the rate at which gases and vapors are released from the surfaces during the outgassing test. This results in the negative values of outgassing rate K. Since the sorbed gases have to be released during pumpdown, the pumpdown time of carbon steel is considerably longer compared with that of stainless steel, aluminum, and copper.

2. Stainless steel, aluminum, and copper show low values of K and a relatively short initial pumpdown time. In particular, the stainless steel also showed a marked reduction in pumpdown time for the second cycle compared with the first cycle.

3. All the painted samples showed a rapid pressure rise during outgassing and a slow pressure drop during pumpdown apparently because of the evaporation of volatile elements. Consequently, the K values for all painted specimens are considerably higher than those of the unpainted metals. In all cases, however, improvements were observed in the subsequent pumpdown cycles. Lower outgassing rates were produced by baked surfaces than by unbaked surfaces. If paint coatings are to be used in vacuum service, it is therefore advisable to apply thin coats first and either vacuum outgas or bake between successive coatings.

Lewis Research Center,
National Aeronautics and Space Administration,
Cleveland, Ohio, October 4, 1965.

APPENDIX - ABSORPTANCE THEORY

In this section is presented an outline of the theory underlying the measurement principles and the data reduction procedures for computing the total normal and total hemispherical absorptances of a sample from the spectral normal reflectance data. Also included is a brief discussion of the variation of reflectances with the sample and source temperatures.

Reflectance Relation

The relation between reflectance, absorptance, and transmittance follows from the law of conservation of energy to give

$$\alpha + \rho + \tau = 1 \tag{A1}$$

where ρ is reflectance, α is absorptance, and τ is transmittance. The above relation holds for both spectral and total radiation. For the materials sufficiently thick to be opaque to incident radiation, equation (1) is simplified to

$$\alpha + \rho = 1 \tag{A2}$$

If a flat sample dA is assumed to be placed in the center of a hemisphere and irradiated diffusely in all directions from the hemispherical blackbody walls, the sample will reflect the incident beams according to its reflectance characteristics.

In figure 9 radiation of intensity $I_{\lambda, B}$ is seen to be incident on a surface at zenith angle θ_i and azimuth angle φ_i. Part of this energy will pass through the surface and be absorbed while the remainder will be reflected, if it is assumed that there is no transmittance. The reflected radiation is in the direction of θ_r, φ_r and has the intensity of I'_λ. The intensity I'_λ may be related to the incident intensity $I_{\lambda, B}$ by the following equation:

$$I_\lambda(\theta_r, \varphi_r) = \int_{\varphi_i} \int_{\theta_i} \rho_\lambda(\theta_i, \varphi_i, \theta_r, \varphi_r) I_{\lambda, B} \sin \theta_i \cos \varphi_i \, d\theta_i \, d\varphi_i \tag{A3}$$

where $\rho_\lambda(\theta_i, \varphi_i, \theta_r, \varphi_r)$ is called bidirectional spectral reflectance since it is related to both the angle of incidence and the angle of reflection. This designation serves to distinguish it from the spectral directional reflectance $\rho_\lambda(\theta_r, \varphi_r)$, which depends on reflectance angles θ_r and φ_r only (ref. 4). Since incident radiant intensity $I_{\lambda, B}$ is constant

at all angles, equation (1) becomes

$$I'_\lambda(\theta_r, \varphi_r) = I_{\lambda, B} \int_{\varphi_i} \int_{\theta_i} \rho_\lambda(\theta_i, \varphi_i, \theta_r, \varphi_r) \sin \theta_i \cos \varphi_i \, d\theta_i \, d\varphi_i \tag{A4}$$

The directional spectral reflectance $\rho_\lambda(\theta_r, \varphi_r)$ is related to the bidirectional spectral reflectance by

$$\rho_\lambda(\theta_r, \varphi_r) = \int_{\varphi_i} \int_{\theta_i} \rho_\lambda(\theta_i, \varphi_i, \theta_r, \varphi_r) \sin \theta_i \cos \varphi_i \, d\theta_i \, d\varphi_i \tag{A5}$$

A perfectly diffuse reflector is one for which the reflected intensity is constant for any angle of incidence. From equation (A5) it can be seen that for a diffuse reflector

$$\rho_\lambda(\theta_r, \varphi_r) = \pi \rho_\lambda(\theta_i, \varphi_i, \theta_r, \varphi_r) \tag{A6}$$

and the intensity of reflected radiation is related to the irradiation by

$$I'_\lambda(\theta_r, \varphi_r) = \rho_\lambda(\theta_r, \varphi_r) I_{\lambda, B} = \rho_\lambda(\theta_i, \varphi_i, \theta_r, \varphi_r) G_{\lambda, B} \tag{A7}$$

where $G_{\lambda, B}$ is the irradiation or the spectral radiant power incident on the surface from all directions.

If the reflector is specular, the bidirectional reflectance is zero for all directions except the direction of the reflected beam. The angle of incidence is equal to the angle of reflection. The intensity of the reflected beam is related to the intensity of the incident beam by the spectral directional reflectance:

$$I'_\lambda(\theta_r, \varphi_r) = \rho_\lambda(\theta_i, \varphi_i) I_{\lambda, B} \tag{A8}$$

and

$$\theta_r = \theta_i, \quad \varphi_r = \varphi_i \pm \pi$$

Spectral normal reflectance is the value of spectral directional reflectance for the case where θ_r equals zero. If normal quantities are denoted with the subscript N, equation (A8) becomes

$$\rho_{\lambda, N} = \frac{I'_{\lambda, N}}{I_{\lambda, B}} \tag{A9}$$

Total directional reflectance is defined as the ratio of total directional intensity of reflected radiation to the total intensity of incident radiation. It is thus defined as

$$\rho_T(\theta_r, \varphi_r) = \frac{\int_\lambda \rho_\lambda(\theta_r, \varphi_r) I_{\lambda, B}\, d_\lambda}{\int_\lambda I_{\lambda, B}\, d_\lambda} \tag{A10}$$

Similarly, the total normal reflectance is

$$\rho_{T, N} = \frac{\int_\lambda \rho_{\lambda, N} I_{\lambda, B}\, d_\lambda}{\int_\lambda I_{\lambda, B}\, d_\lambda} \tag{A11}$$

Spectral hemispherical reflectance is calculated by integrating the reflected intensity I'_λ over the hemisphere and by taking a ratio to the spectral radiant power $G_{\lambda, B}$:

$$\rho_{\lambda, H} = \frac{I_{\lambda, B}}{G_{\lambda, B}} \int_{\varphi_r} \int_{\theta_r} \rho_\lambda(\theta_r, \varphi_r) \sin \theta_r \cos \varphi_r\, d\theta_r\, d\varphi_r \tag{A12}$$

Similarly, total hemispherical reflectance is obtained by

$$\rho_{T, H} = \frac{1}{G_B} \int_\lambda \int_{\varphi_r} \int_{\theta_r} \rho_\lambda(\theta_r, \varphi_r) I_{\lambda, B} \sin \theta_r \cos \varphi_r\, d\theta_r\, d\varphi_r\, d_\lambda \tag{A13}$$

where G_B is the total radiant power.

In the actual test in which a heated reflectometer (hohlraum) was used, a spectral normal reflectance $\rho_{\lambda, N}$ is obtained by measuring the incident and reflected intensities $I_{\lambda, B}$ and $I'_{\lambda, N}$. From these data, total normal reflectance $\rho_{T, N}$ can be obtained by integrating graphically over the range of λ corresponding to the wavelength range over which the data is obtained:

$$\rho_{T, N} = \frac{\int_{\lambda_1}^{\lambda_2} \rho_{\lambda, N} I_{\lambda, B}\, d_\lambda}{\int_{\lambda_1}^{\lambda_2} I_{\lambda, B}\, d_\lambda} \tag{A14}$$

Relation Between Normal and Hemispherical Reflectance

Equations (A12) and (A13) show that to calculate the hemispherical reflectances from normal reflectance data obtained by experiments, directional variation of reflectance must be known. Usually, such information is not available.

The ratio of total normal and total hemispherical absorptances of electrical conductors and nonconductors of smooth isotropic surfaces has been calculated and compared with experimental values in reference 11. The above reference indicates that the ratio of total hemispherical absorptance and total normal absorptance varies from 1.33 to 1.05 for conductors and from 1.05 to 0.95 for nonconductors. Most metallic surfaces in engineering applications are not smooth and pure but are generally covered with thin oxide films. Since oxides are dielectric, absorptances of metal surfaces become a function of the properties of the two materials, dielectric oxides and electric conductors. If the metal surfaces are painted, the pigment and binder are mostly of dielectric nature. It was assumed therefore in this report that the total hemispherical absorptance is equal to the total normal absorptance for most of the metals, painted or unpainted, in the engineering applications.

Variation of Reflectance With Temperature

The spectral reflectivity of a dielectric material in air is directly related to the index of refraction for normal incidence by Fresnel's equation (ref. 12):

$$\rho_\lambda = \left(\frac{n_\lambda - 1}{n_\lambda + 1}\right)^2 \tag{A15}$$

where n_λ is the index of refraction. The index of refraction is a function of the coefficient of thermal expansion of the dielectric, which is generally small. Therefore, the effect of temperature on the spectral reflectivity should also be small. This suggests that spectral reflectance measurements made at room temperature on nonconductors may be used for other temperatures without large errors.

In the case of a metal electric conductor with a smooth surface, the spectral reflectivity of the normal incident beam for the infrared wavelength region is expressed by the Hagen-Rubens equation (ref. 13)

$$\rho_\lambda = 1 - \alpha_\lambda = 1 - 36.05\sqrt{\frac{\gamma}{\lambda}} \tag{A16}$$

for temperatures below 700° F, where γ is the specific volume resistivity, in $(\Omega)(cm)$, and λ is the wavelength in μ. For many pure metals, the specific volume resistivity is approximately proportional to the absolute temperature; therefore, the spectral absorptivity α_{λ} is approximately proportional to the square root of the absolute temperature.

Total reflectances are not only affected by the sample (receiver) temperature but also by the temperature of the source of incident radiation. The source temperature determines the spectral distribution of incident intensity. The relation may be seen clearly if equation (A11) is rewritten as follows

$$\rho_{T,N}(T_R, T_B) = \frac{\int_{\lambda_1}^{\lambda_2} \rho_{\lambda,N}(T_R) I_{\lambda,B}(T_B) d\lambda}{\int_{\lambda_1}^{\lambda_2} I_{\lambda,B}(T_B) d\lambda} \tag{A17}$$

where T_R is the receiver temperature and T_B is the blackbody source temperature. It is noted that the total normal reflectance is a function of both T_R and T_B.

In general, the total reflectance increases with the source temperature for dielectric materials and decreases for conductors (ref. 14).

The total normal reflectance for different source temperatures may be calculated by graphical integration of equation (A11) if the functional relation of $I_{\lambda,B}$ and λ is noted to be different for different temperatures. The values of blackbody intensity $I_{\lambda,B}$ for different values of λ at a given temperature T_B are tabulated in reference 8.

Total Normal and Total Hemispherical Absorptances

From the spectral normal reflectance values, which are obtained from experiments over a wavelength range of λ_1 and λ_2, total normal absorptance $\alpha_{\lambda,N}$ over the same wavelength range can be calculated by using relations (A2) and (A14):

$$\alpha_{T,N} = \frac{\int_{\lambda_1}^{\lambda_2} (1 - \rho_{\lambda,N}) I_{\lambda,B}\, d\lambda}{\int_{\lambda_1}^{\lambda_2} I_{\lambda,B}\, d\lambda} \tag{A18}$$

Spectral distribution of blackbody radiation intensity $I_{\lambda, B}$ required to complete the integrations is obtainable from published data such as given in reference 14. Total hemispherical absorptance may be calculated in a similar manner by using relations (A2) and (A13) if the spectral directional reflectance $\rho_\lambda(\theta_r, \varphi_r)$ is known:

$$\alpha_{T, H} = \frac{1}{G_B} \int_\lambda \int_{\varphi_r} \int_{\theta_r} \left[1 - \rho_\lambda(\theta_r, \varphi_r)\right] I_{\lambda, B} \sin \theta_r \cos \varphi_r \, d\theta_r \, d\varphi_r \, d_\lambda \tag{A19}$$

Usually, data on spectral directional reflectance are either not available or difficult to obtain by experiments. For the reasons mentioned previously, however, the total hemispherical absorptance may be assumed without much error equal to the total normal absorptance for most engineering applications.

Total Hemispherical Emittance

Total hemispherical emittance is calculated by use of Kirchhoff's Law, which states that if the temperature of a source of incident radiation and that of a receiver is identical, total hemispherical absorptance $\alpha_{T, H}$ is equal to total hemispherical emittance $\epsilon_{T, H}$.

As previously mentioned (in the section, Variation of Reflectance With Temperature) for electric nonconductors the absorptance may be assumed without much error to be independent of the temperature of the receiver; therefore, the total hemispherical emittance may be calculated from a known total hemispherical absorptance by use of the following relation:

$$\epsilon_{T, H}(T_B) = \frac{\int_{\lambda_1}^{\lambda_2} \alpha_{\lambda, H} I_{\lambda, B}(T_B) \, d_\lambda}{\int_{\lambda_1}^{\lambda_2} I_{\lambda, B}(T_B) d_\lambda} \tag{A20}$$

This indicates that the total hemispherical emittance is equal to the total hemispherical absorptance obtained for a source temperature T_B without regard to the receiver temperature T_R.

REFERENCES

1. Lengyel, A.; Marfone, P. A.; and Santeler, D. J.: Design Criteria for a Space Environment Simulator. Paper No. 61-AV-52, ASME, 1961.

2. Dayton, B. B.: Relations Between Size of Vacuum Chamber, Outgassing Rate, and Required Pumping Speed. 1959 Nat. Vacuum Symposium Trans., Am. Vacuum Soc., 1960, pp. 101-119.

3. Lieblein, Seymour: Heat Transfer Aspects of Space Radiators. NASA TP-5-63, 1963.

4. Dunkle, R. V.: Thermal Radiation Characteristics of Surfaces. Theory and Fundamental Research in Heat Transfer, Pergamon Press, 1963, pp. 1-31.

5. Dunkle, Robert V.: Spectral Reflectance Measurements. First Symposium - Surface Effects on Spacecraft Materials, F. J. Clauss, ed., John Wiley & Sons, Inc, 1960, pp. 117-137.

6. Anon.: Infrared Equipment Instruction Manuals Numbers 990-9004 and 990-9188. Perkin-Elmer Corp.

7. Streed, E. R.; McKellar, L. A.; Rolling, R., Jr.; and Smith, C. A.: Errors Associated with Hohlraum Radiation Characteristics Determinations. Vol. 1 of Symposium on Measurement of Thermal Radiation Properties of Solids, Dayton (Ohio), Sept. 5-7, 1962, pp. 11-74 - 11-104.

8. Eckert, E. R. G.; and Drake, R. M., Jr.: Heat and Mass Transfer. McGraw-Hill Book Co., Inc., 1959.

9. Kruse, P. W., et al.: Elements of Infrared Technology. John Wiley & Sons, Inc., 1962.

10. Dushman, S.: Scientific Foundations of Vacuum Technique. John Wiley & Sons, Inc., 1949.

11. Jakob, M.: Heat Transfer. John Wiley & Sons, Inc., 1957.

12. Bevans, J. T.; Gier, J. T.; and Dunkle, R. V.: Comparison of Total Emittances with Values Computed from Spectral Measurements. Trans. ASME, vol. 80, no. 7, Oct. 1958, pp. 1405-1416

13. Snyder, N. W.: Radiation in Metals. Trans. ASME, vol. 76, no. 4, May 1954, pp. 541-548.

14. Dunkle, R. V : Thermal-Radiation Tables and Applications. Trans. ASME, vol. 76, no. 4, May 1954, pp. 549-552.

TABLE I. - TEST SPECIMENS FOR THERMAL RADIATION ABSORPTANCE

(a) Surface coatings

Specimen	Description	Manufacturer
1	Missile black, no. RGL-22818	Glidden Co.
2	Missile white, no. RGL-22576	Glidden Co.
3	Black lacquer, no. 9099	Glidden Co.
4	White lacquer	Illinois Bronze Powder Co.
5	Rust-Oleum clear, no. 200	Rust-Oleum Corp.
6	Rust-Oleum white, no. 225	Rust-Oleum Corp.
7	Rust-Oleum silver gray, no. 208	Rust-Oleum Corp.
8	Rust-Oleum red, no. 215	Rust-Oleum Corp.
9	Rust-Oleum green, no. 205	Rust-Oleum Corp.
10	Glyptal red enamel, no. 1201	General Elec. Co.
11	Zinc chromate primer, no. 960	Rust-Oleum Corp.
12	15 parts zinc chromate plus 1 part missile black	Same as for specimens 1 and 11
13	Nylon on white lacquer, 15-weight-percent solution in ethyl alcohol[a]	Du Pont Co.
14	Nylon on zinc chromate, 15-weight-percent solution in ethyl alcohol[a]	Du Pont Co.
15	Nylon on vapor-blasted 316 stainless steel, 15-weight-percent solution in ethyl alcohol[a]	Du Pont Co.
16	White porcelain enamel	Magic Iron Cement Co.

[a]Nylon coating thickness, av 2 mils.

TABLE I. - Concluded. TEST SPECIMENS FOR THERMAL RADIATION ABSORPTANCE

(b) Oxidized AISI 316 stainless steel

Specimen	Sandblast grit	Oxidation temperature, °F	Oxidation time, hr	Specimen	Sandblast grit	Oxidation temperature, °F	Oxidation time, hr
1	[a]325	1200	1	19	325	1400	24
2	[b]80	1200	1	20	80	1400	24
3	325	1200	4	21	325	1600	1
4	80	1200	4	22	80	1600	1
5	325	1200	8	23	325	1600	4
6	80	1200	8	24	80	1600	4
7	325	1200	16	25	325	1600	8
8	80	1200	16	26	80	1600	8
9	325	1200	24	27	325	1600	16
10	80	1200	24	28	80	1600	16
11	325	1400	1	29	325	1600	24
12	80	1400	1	30	80	1600	24
13	325	1400	4	31	325	1800	2
14	80	1400	4	32	80	1800	2
15	325	1400	8	33	325	1800	6
16	80	1400	8	34	80	1800	6
17	325	1400	16	35	[c]40	1800	16
18	80	1400	16	36	40	1800	24

[a]Surface roughness, av 22 to 25 μin.

[b]Surface roughness, av 60 to 62 μin.

[c]Surface roughness, av 220 to 250 μin.

TABLE II. - CALCULATED TOTAL NORMAL ABSORPTANCE FOR PAINTED SURFACES

Specimen	Description	Source temperature, ^{o}F	
		1112	1500
		Total normal absorptance, $\alpha_{T,N}$	
1	Missile black	0.92	0.94
2	Missile white	.80	.76
3	Black lacquer	.92	.94
4	White lacquer	.79	.73
5	Rust-Oleum clear	.85	.82
6	Rust-Oleum white	.89	.84
7	Rust-Oleum silver gray	.90	.88
8	Rust-Oleum red	.86	.80
9	Rust-Oleum green	.82	.77
10	Glyptal	.80	.75
11	Zinc chromate primer	.84	.79
12	15 parts zinc chromate plus 1 part missile black	.75	.84
13	Nylon on white lacquer	.88	.84
14	Nylon on zinc chromate	.86	.84
15	Nylon on vapor-blasted 316 stainless steel	.70	.70
16	White porcelain enamel	.79	.74

TABLE III. - SPECTRAL NORMAL REFLECTANCE FOR AISI 316 STAINLESS STEEL OXIDIZED AT 1400° and 1600° F

Wavelength, μ	Grit									
	325	80	325	80	325	80	325	80	325	80
	Oxidation time, hr									
	1	1	4	4	8	8	16	16	24	24
	Spectral normal reflectance, $\rho_{\lambda, N}$, percent									
AISI 316 stainless steel oxidized at 1400° F										
2	27	24	12	21	30	23	35	27	25	26
3	30	25	12	23	34	24	37	30	24	26
4	33	27	14	25	37	27	43	35	28	31
5	40	31	21	28	46	31	50	41	36	36
6	43	35	35	33	52	32	57	43	40	37
7	47	40	43	38	57	33	62	45	40	38
8	49	41	47	39	52	29	60	42	37	35
9	48	39	54	37	43	20	53	32	31	29
10	53	34	60	37	51	24	59	35	39	30
11	60	43	65	41	55	24	63	39	51	36
12	65	47	70	46	56	24	65	37	59	40
13	69	51	74	48	57	26	69	32	69	47
14	68	52	74	49	47	22	65	32	67	50
15	60	49	73	45	41	22	65	32	62	48
AISI 316 stainless steel oxidized at 1600° F										
2	28	25	24	27	19	20	19	19	16	20
3	30	27	22	31	20	23	21	20	17	22
4	34	23	20	32	21	25	21	16	17	21
5	37	31	21	36	23	28	23	20	19	23
6	43	36	23	43	27	32	26	19	21	26
7	50	42	26	45	31	35	30	23	24	27
8	55	44	28	41	30	32	27	24	24	24
9	59	43	27	26	27	25	27	18	17	16
10	66	42	28	29	27	25	27	19	18	19
11	75	48	38	34	39	30	31	21	22	23
12	81	53	52	41	54	36	41	24	31	24
13	84	55	66	46	67	42	57	26	50	25
14	76	55	52	43	67	41	56	28	54	26
15	69	54	36	44	59	39	46	31	50	28

TABLE IV. - CALCULATED TOTAL NORMAL ABSORPTANCE FOR AISI 316 STAINLESS STEEL OXIDIZED AT 1800° F

Specimen	Oxidation time, hr	Source temperature, °F	
		1112	1500
		Total normal absorptance, $\alpha_{T,N}$	
32	2	0.86	0.85
34	6	.82	.81
35	16	.88	.88
36	24	.84	.84

TABLE V. - TEST SPECIMENS FOR OUTGASSING RATE

Specimen	Description	Treatment	Specimen size, in.	
			Outside diameter	Length
1	Severely rusted carbon steel, ASTM A53, standard pipe from stock	Vapor degreased, placed outdoors 1 week	16	16
2	Slightly rusted carbon steel, ASTM A53, standard pipe from stock	Vapor degreased, placed outdoors 3 days	16	16
3	Carbon steel, ASTM A53, standard pipe from stock (sample 1)	Sand blasted with Grit 80	14	12
4	Carbon steel, same as for specimen 3 (sample 2)	Sand blasted with Grit 80 and vapor degreased	16	16
5	AISI 304 Stainless steel from stock	Vapor degreased and exposed to atmosphere (indoor) 1/2 day, as-received surface	14	12
6	Aluminum, type unknown	Cleaned with alcohol, as-received surface	14	12
7	Copper, type unknown	Cleaned with alcohol, as-received surface	14	12
8	Glyptal, General Electric Co. no. 1201 (sample 1)	Mixture of 2 parts Glyptal and 1 part thinner, sprayed to 1.5 mils dried in air for 1 week	16	16
9	Glyptal, no. 1201 (sample 2)	Same as for specimen 8 but baked 4 hr at 125° F	16	16
10	Glyptal, no. 1201 (sample 3)	Sprayed to 4 mils dried in air 24 hr	14	12

TABLE V. - Continued. TEST SPECIMENS FOR OUTGASSING RATE

Specimen	Description	Treatment	Specimen size, in.	
			Outside diameter	Length
11	Glyptal, no. 1201 (sample 4)	Sprayed to 4 mils, baked 4 hr at 125° F	14	12
12	Missile black, Glidden Co. no. RGL-22818 (sample 1)	1.5 Mils primer, 1.5 mils finish sprayed, dried in air 24 hr	14	12
13	Same as for specimen 12 (sample 2)	Same as for specimen 12, but baked 4 hr at 125° F	14	12
14	Rust-Oleum clear, no. 200 (sample 1)	Brush applied to 1.5 mils, dried in air 24 hr	14	12
15	Rust-Oleum clear, no. 200 (sample 2)	Same as for specimen 14, but baked 4 hr at 150° F	14	12
16	Rust-Oleum clear, no. 200 (sample 3)	Same as for specimen 14, but baked 4 hr at 150° F, then exposed to air 24 hr	14	12
17	Rust-Oleum red primer, no. 215	Brush applied to 1.5 mils, dried in air 24 hr	14	12
18	Rust-Oleum green, no. 205, on red primer, no. 215 (sample 1)	Each brush applied to 1.5 mils, dried in air 24 hr	14	12
19	Same as for specimen 18 (sample 2)	Same as for specimen 18, but baked 4 hr at 150° F	14	12
20	Rust-Oleum white, no. 205, on green, no. 215 (sample 1)	Each brush applied to 1.5 mils, dried in air 24 hr	14	12

TABLE V. - Concluded. TEST SPECIMENS FOR OUTGASSING RATE

Specimen	Description	Treatment	Specimen size, in.	
			Outside diameter	Length
21	Same as for specimen 20 (sample 2)	Same as for specimen 20, but baked 4 hr at 125° F	14	12
22	Rust-Oleum gray, no. 208	Brush applied to 1.5 mils	16	16
23	Rust-Oleum white, no. 225	Brush applied to 1.5 mils	16	16
24	Phenoline, Carboline Co. (sample 1)	Brush applied, phenoline 305 primer, 4 mils; phenoline 305 finish, 4 mils	14	12
25	Phenoline, Carboline Co. (sample 2)	Brush applied, epoxy 190 primer, 3 mils; epoxy X2191-31 finish, 7 to 8 mils; total 10 to 11 mils		
26	Zinc chromate, Rust-Oleum, no. 960	Brush applied to approx 1.5 mils	14	12
27	White porcelain enamel, Magic Iron Cement Co.	Sprayed to approx 1.5 mils	14	12
28	White lacquer, Illinois Bronze Powder Co., no. 17875	Sprayed to approx 1.5 mils	14	12
29	Du Pont nylon, 15-weight-percent solution in ethyl alcohol	Three coats brush applied to approx 2 mils, cured at 150° F immediately after coating	14	12

TABLE VI. - OUTGASSING RATE, OUTGASSING INDEX, AND DIFFERENTIAL TIME FOR SURFACE COATINGS AND METALS

Specimen	Description	Outgassing rate, K, $\frac{(torr)(liter)}{(sec)(cm^2)}$		Outgassing index				Differential time, Δt, min	
				a		b			
		Cycle							
		First	Second	First	Second	First	Second	First	Second
	Typical empty bell jar	0	0	3.6×10^5	2.1×10^5	1.055	1.070	23.0	37.0
1	Severely rusted carbon steel	-1.04×10^7	-1.49×10^7	7.0	3.0	.705	.690	43.0	160.0
2	Slightly rusted carbon steel	-3.53	-2.35	1.8	2.1	.740	.658	220.0	340.0
3	Carbon steel, sample 1	.03	-.05	8.5	1.2	.989	.851	12.0	12.0
4	Carbon steel, sample 2	-.01	-.04	4.0	2.3	.996	.975	25.0	48.0
5	Stainless steel	.01	.01	4.7	4.0	1.125	1.040	15.0	22.0
6	Aluminum	.04	-----	8.5	----	1.010	-----	12.0	-----
7	Copper	.05	-----	7.2	----	1.055	-----	12.0	-----
8	Glyptal, sample 1	.86	.63	44.0	35.0	.936	.955	2.4	3.0
9	Glyptal, sample 2	.77	.84	55.0	48.0	.865	.926	2.0	2.2
10	Glyptal, sample 3	.79	.84	40.0	37.0	1.040	1.080	2.4	2.5
11	Glyptal, sample 4	.41	.24	22.0	12.0	1.085	1.320	4.0	5.0
12	Missile black, sample 1	1.03	.98	20.0	40.0	1.742	1.090	2.6	2.3
13	Missile black, sample 2	.71	.06	90.0	10.0	1.050	.900	1.1	13.0
14	Rust-Oleum clear, sample 1	.50	.51	30.0	25.0	1.310	1.340	2.5	2.8
15	Rust-Oleum clear, sample 2	.41	.41	19.0	18.0	1.200	1.120	4.2	4.6
16	Rust-Oleum clear, sample 3	.23	.87	12.0	----	1.150	-----	6.2	-----
17	Rust-Oleum red primer	.87	.87	35.0	32.0	1.260	1.250	2.3	2.6
18	Rust-Oleum green on red, sample 1	.50	-----	18.0	----	1.280	-----	3.8	-----
19	Rust-Oleum green on red, sample 2	1.38	.03	62.0	5.0	1.080	1.020	1.6	19.0
20	Rust-Oleum white on green, sample 1	1.17	.29	64.0	10.0	.935	.895	1.6	6.2
21	Rust-Oleum white on green, sample 2	1.08	.08	60.0	5.5	.962	1.130	1.8	13.0
22	Rust-Oleum gray	1.15	.56	76.0	29.0	.802	1.030	1.4	3.4
23	Rust-Oleum white	.96	.93	90.0	45.0	1.050	1.010	1.1	2.2
24	Phenoline, sample 1	-----	-----	----	----	-----	-----	----	-----
25	Phenoline, sample 2	-----	-----	----	----	-----	-----	----	-----
26	Zinc chromate	1.20	.11	56.0	9.0	1.095	1.000	1.7	11.0
27	White porcelain	.86	-----	45.0	----	1.015	-----	2.2	-----
28	White lacquer	.29	-----	15.0	----	1.000	1.000	6.7	-----
29	Nylon	1.84	.11	82.0	----	1.100	-----	1.2	-----

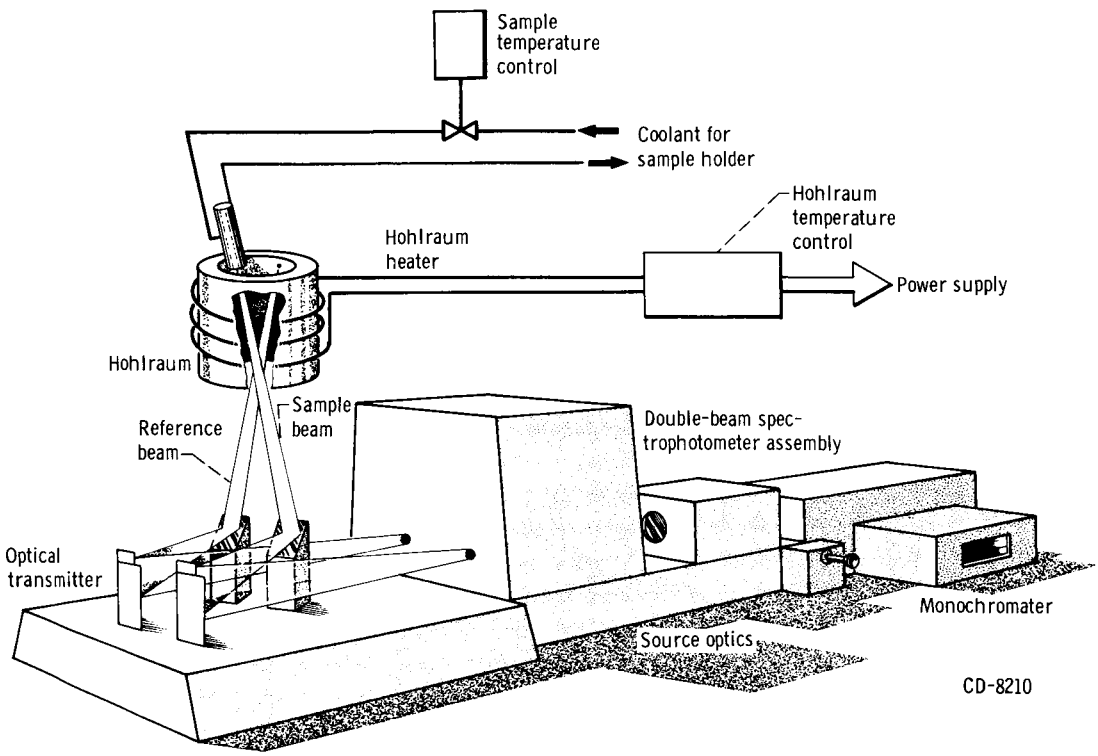

Figure 1. - Schematic view of spectrophotometer and hohlraum.

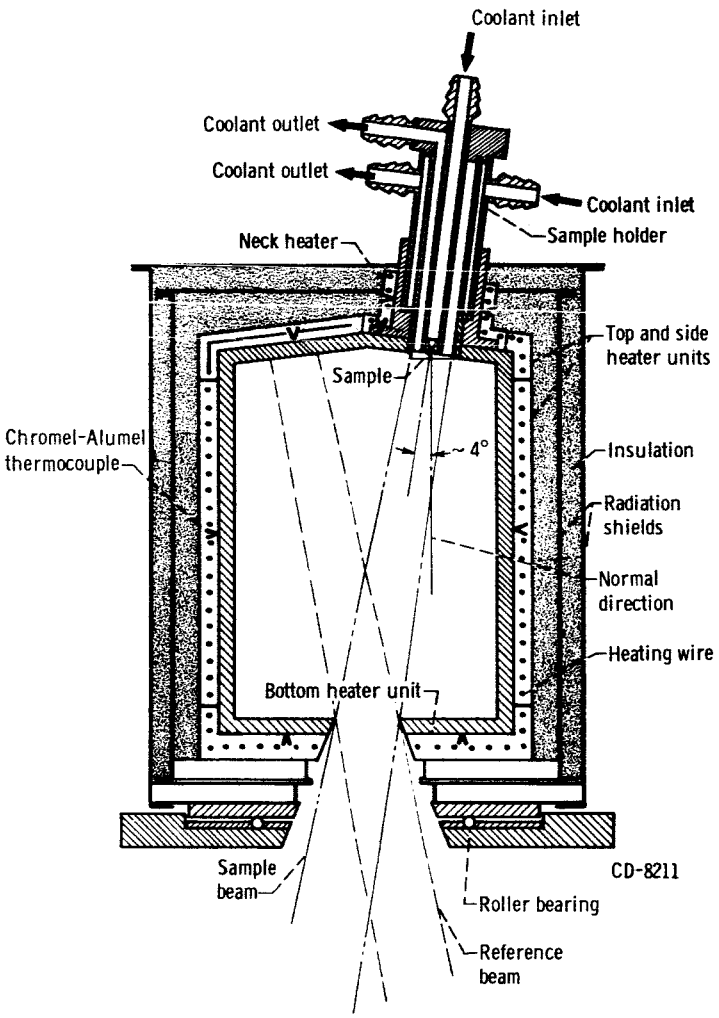

Figure 2. - Detail of hohlraum.

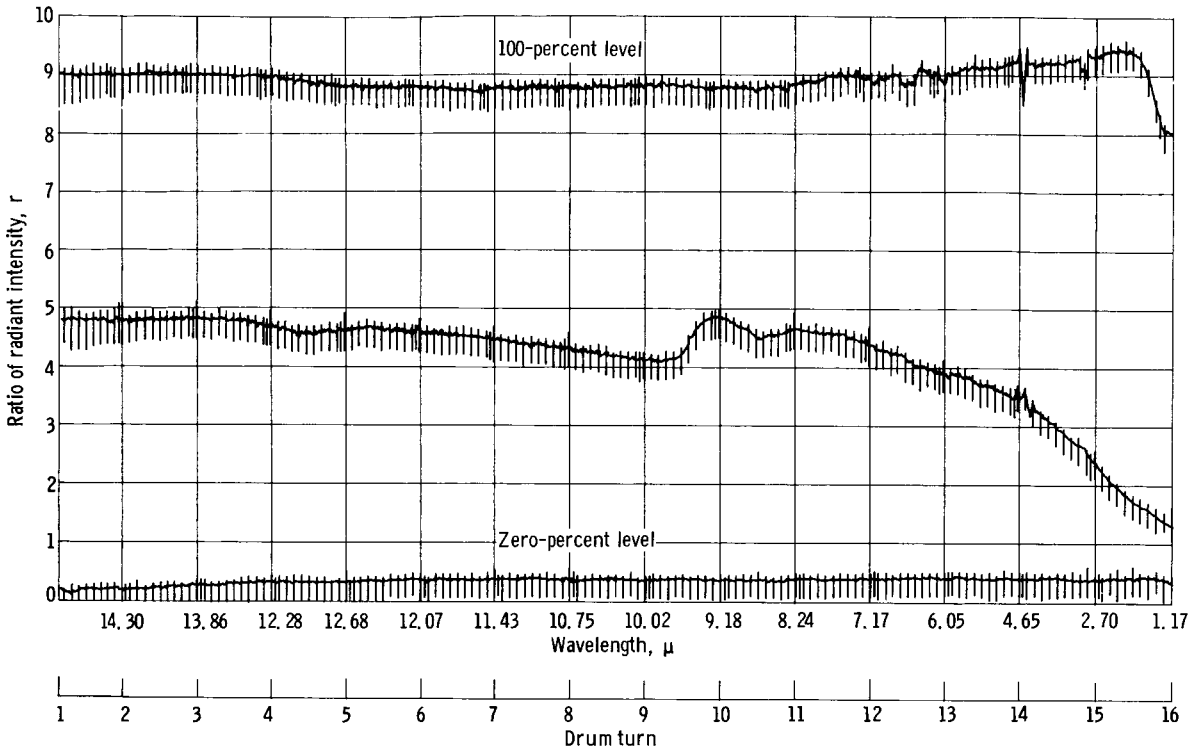

Figure 3. - Typical hohlraum chart recording

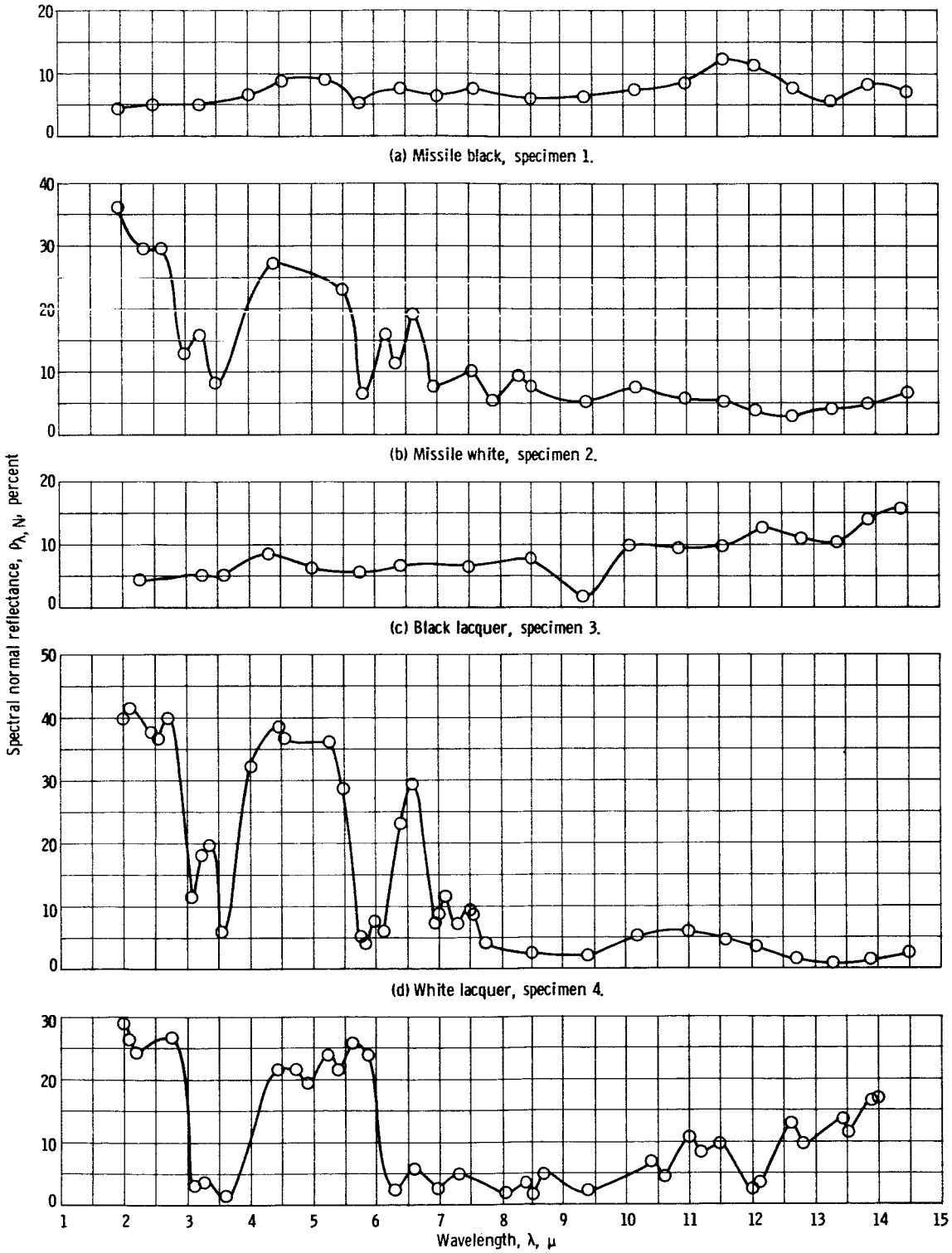

Figure 4. - Spectral normal reflectance of coated surfaces (data taken from table I(a)).

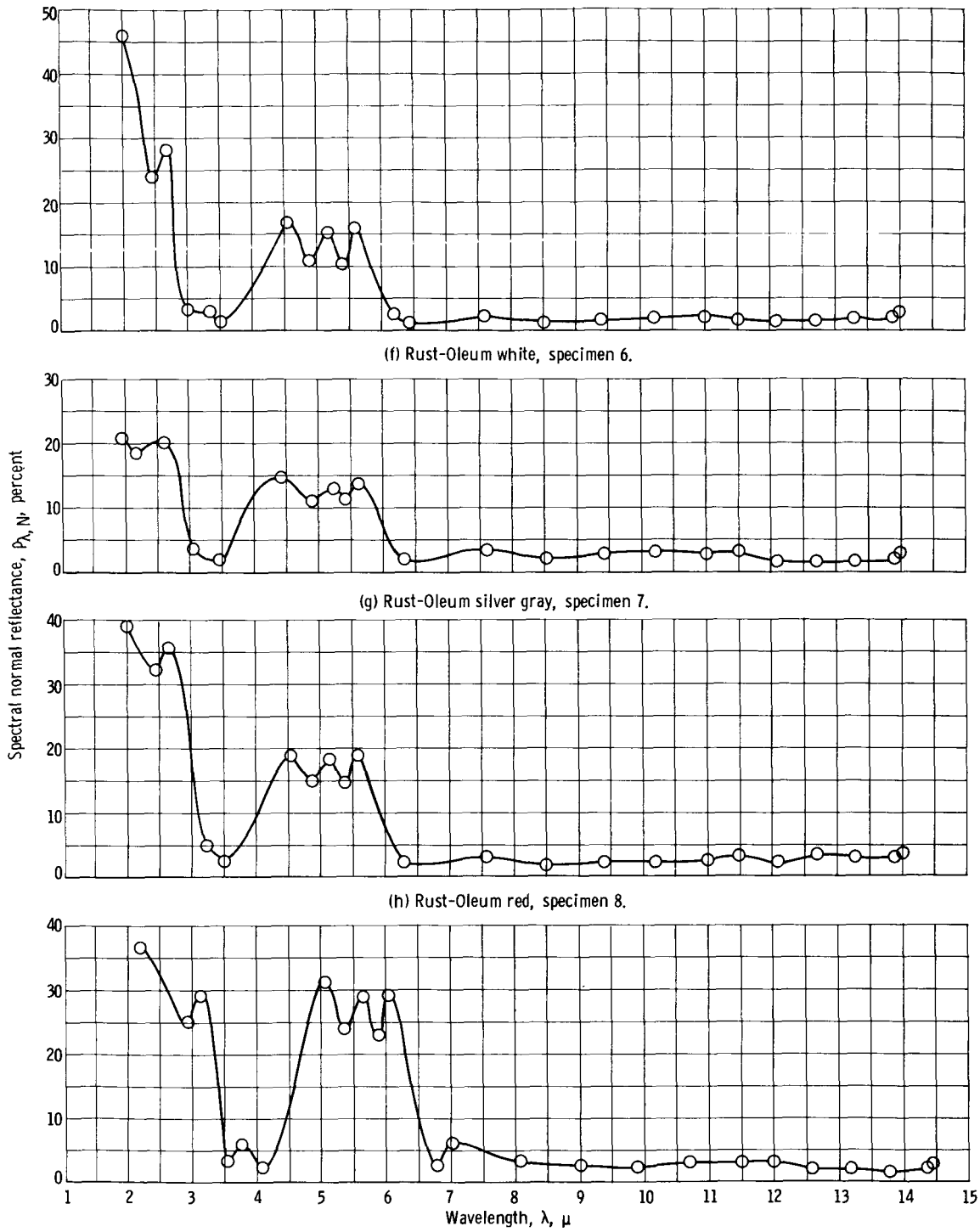

(f) Rust-Oleum white, specimen 6.

(g) Rust-Oleum silver gray, specimen 7.

(h) Rust-Oleum red, specimen 8.

(i) Rust-Oleum green, specimen 9.

Figure 4. - Continued.

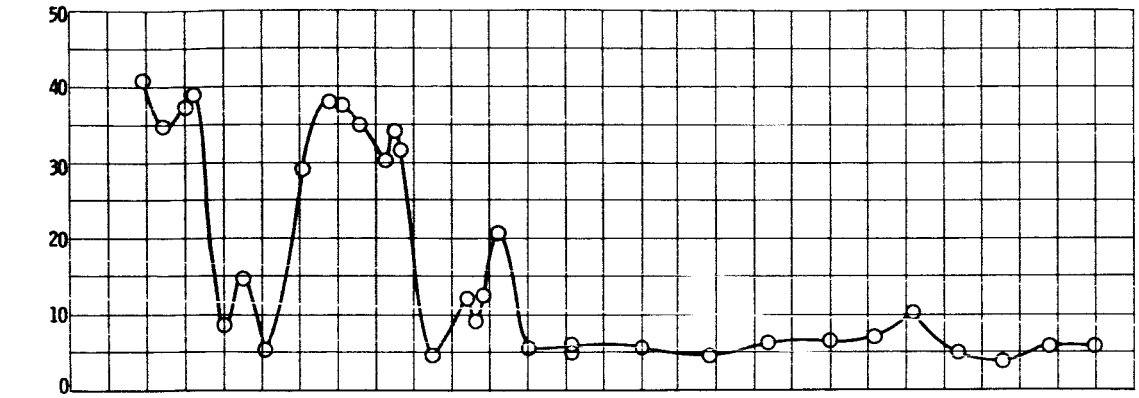

(j) Red Glyptal, specimen 10.

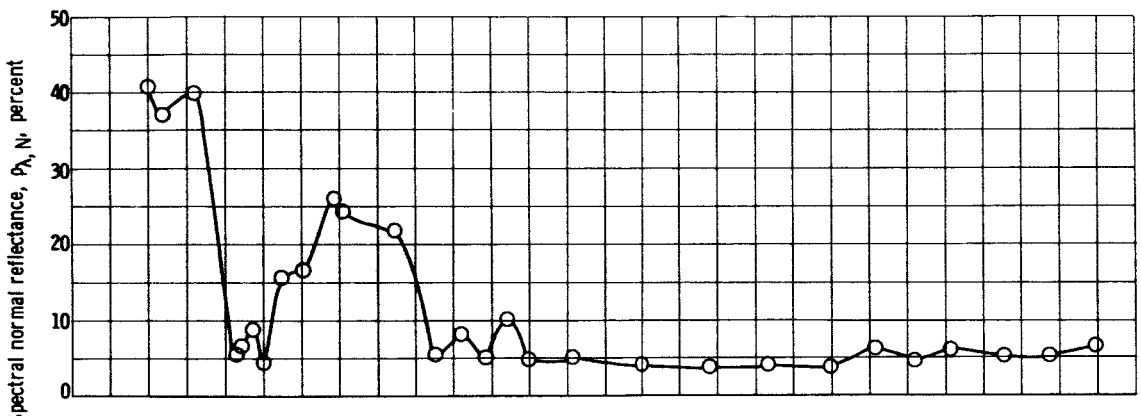

(k) Zinc chromate, specimen 11.

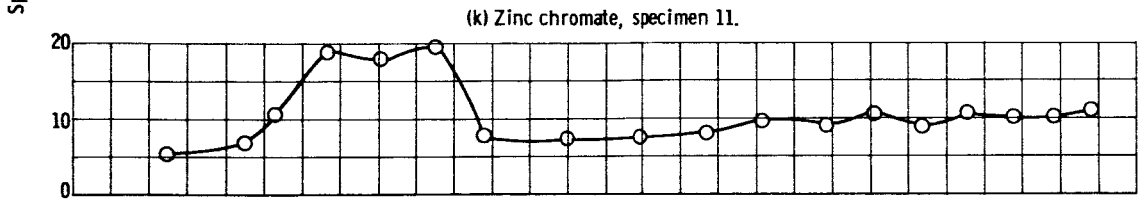

(l) Mixture of fifteen parts zinc chromate and one part missile black, specimen 12.

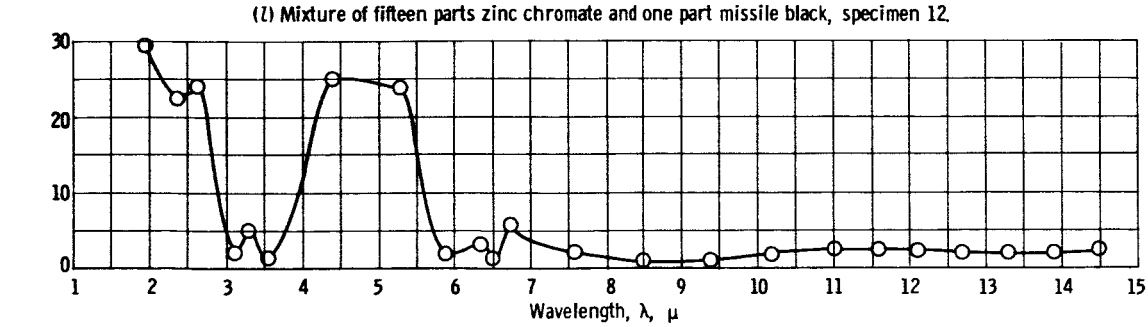

(m) Nylon on white lacquer, specimen 13.

Figure 4. - Continued.

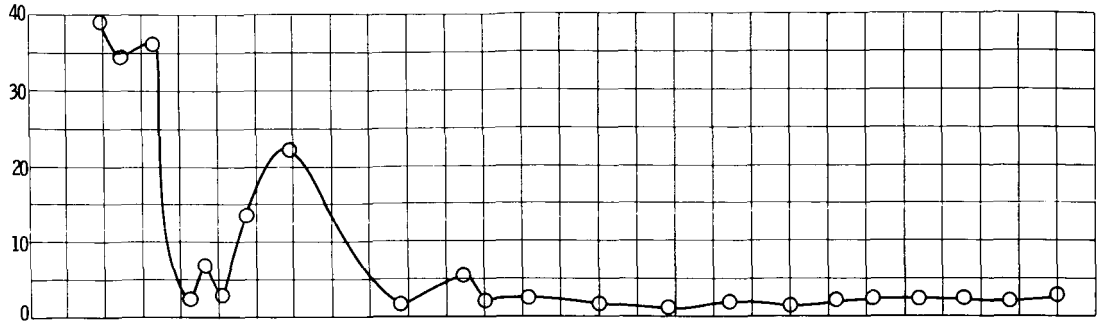

(n) Nylon on zinc chromate, specimen 14.

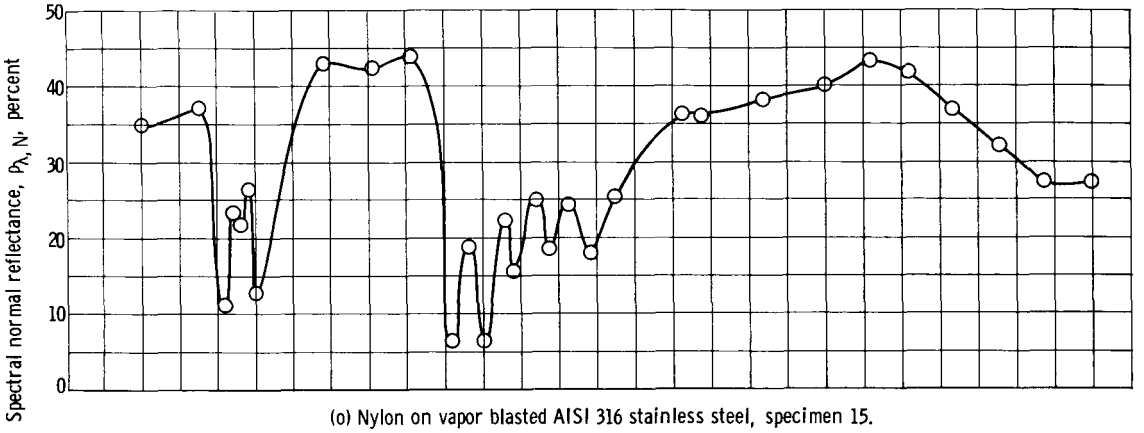

(o) Nylon on vapor blasted AISI 316 stainless steel, specimen 15.

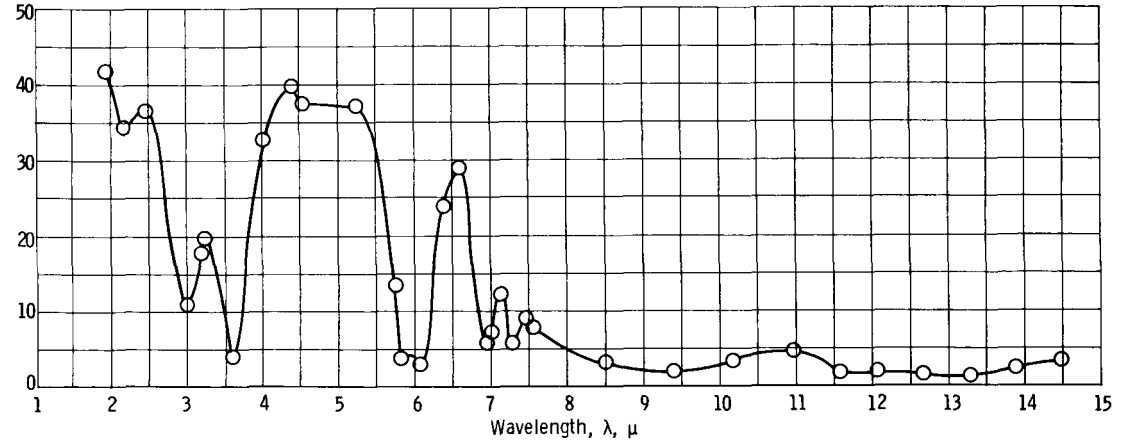

(p) White porcelain enamel, specimen 16.

Figure 4. - Concluded.

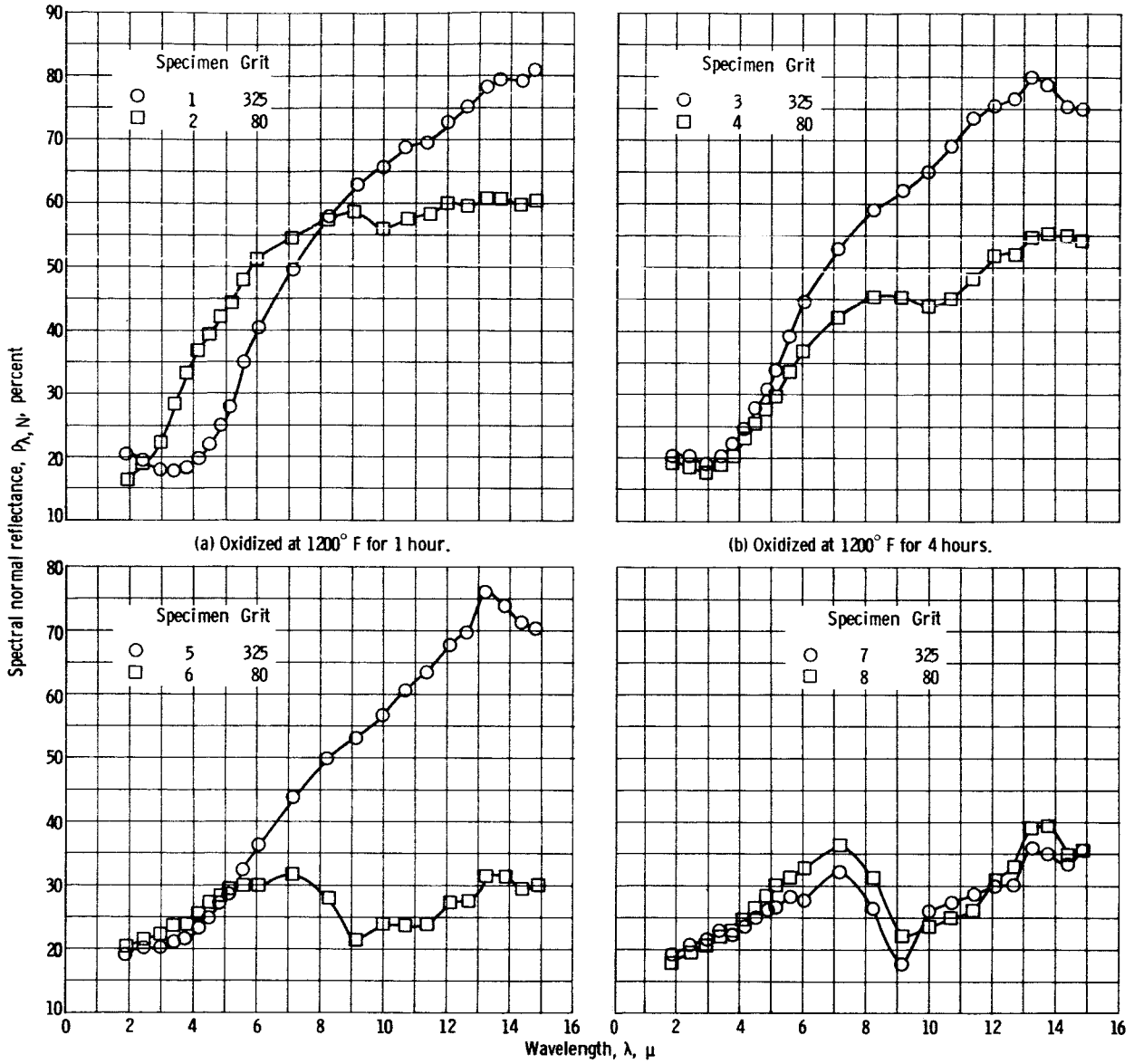

(a) Oxidized at 1200° F for 1 hour.

(b) Oxidized at 1200° F for 4 hours.

(c) Oxidized at 1200° F for 8 hours.

(d) Oxidized at 1200° F for 16 hours.

Figure 5. - Spectral normal reflectance of oxidized AISI 316 stainless steel.

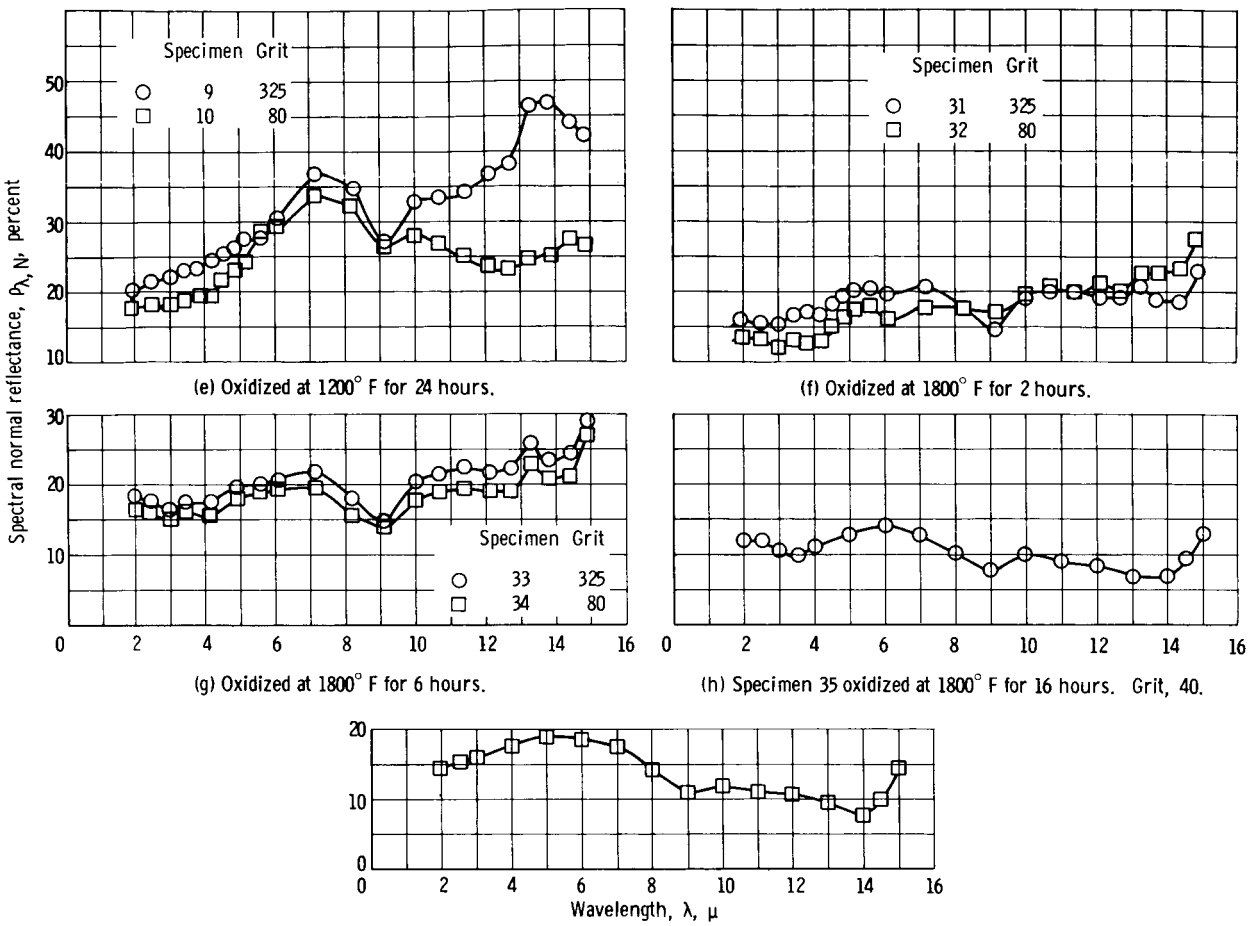

(e) Oxidized at 1200° F for 24 hours.

(f) Oxidized at 1800° F for 2 hours.

(g) Oxidized at 1800° F for 6 hours.

(h) Specimen 35 oxidized at 1800° F for 16 hours. Grit, 40.

(i) Specimen 36 oxidized at 1800° F for 24 hours. Grit, 40.

Figure 5. - Concluded.

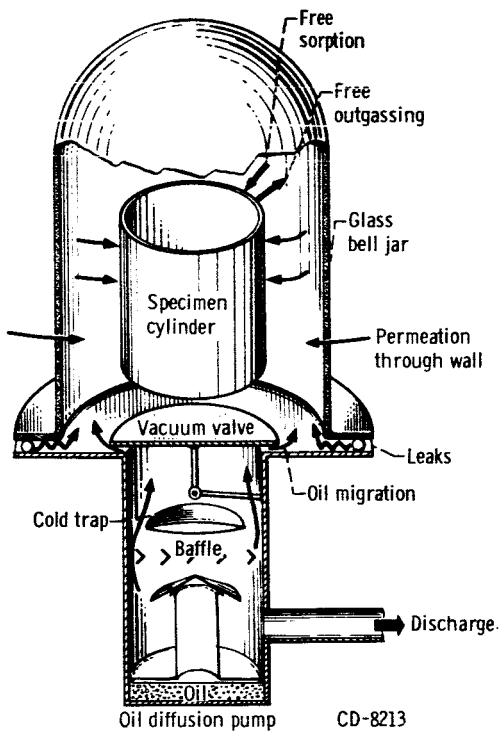

Figure 6. - Schematic drawing showing material balance in bell jar vacuum system.

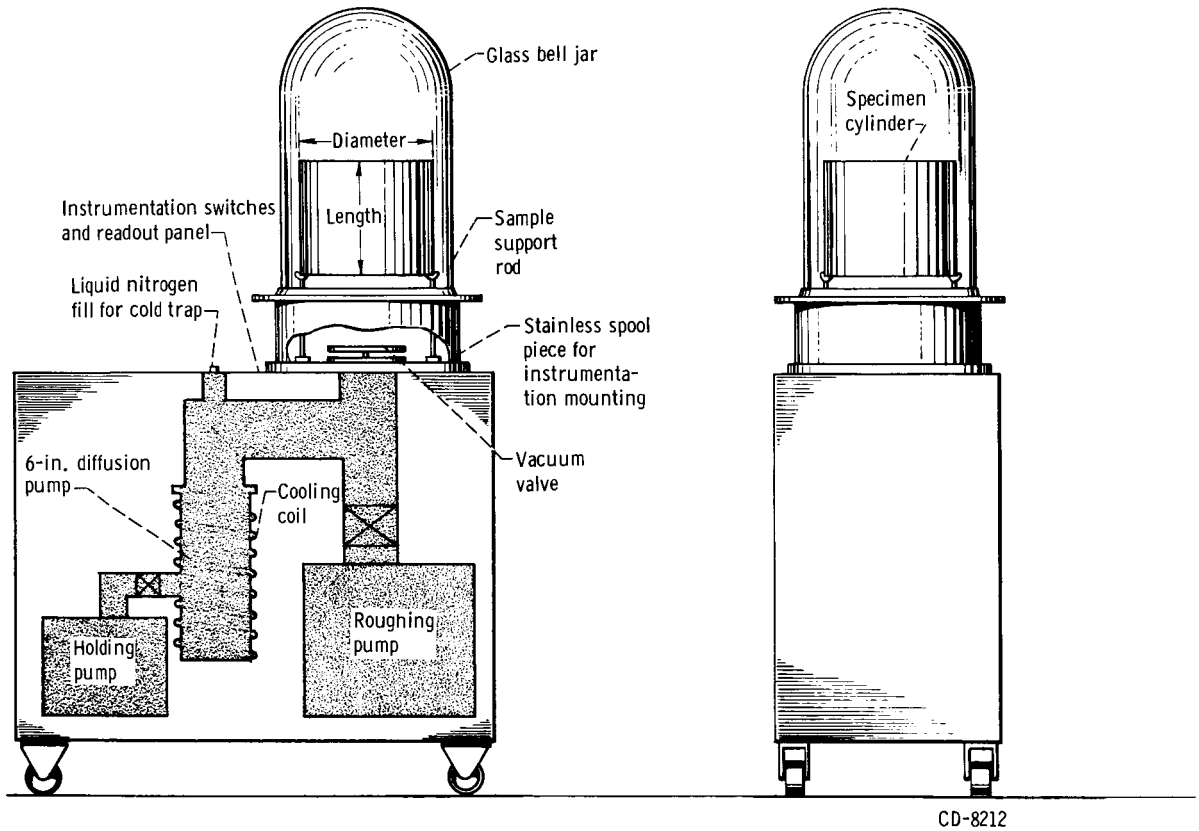

Figure 7. - Bell jar vacuum system.

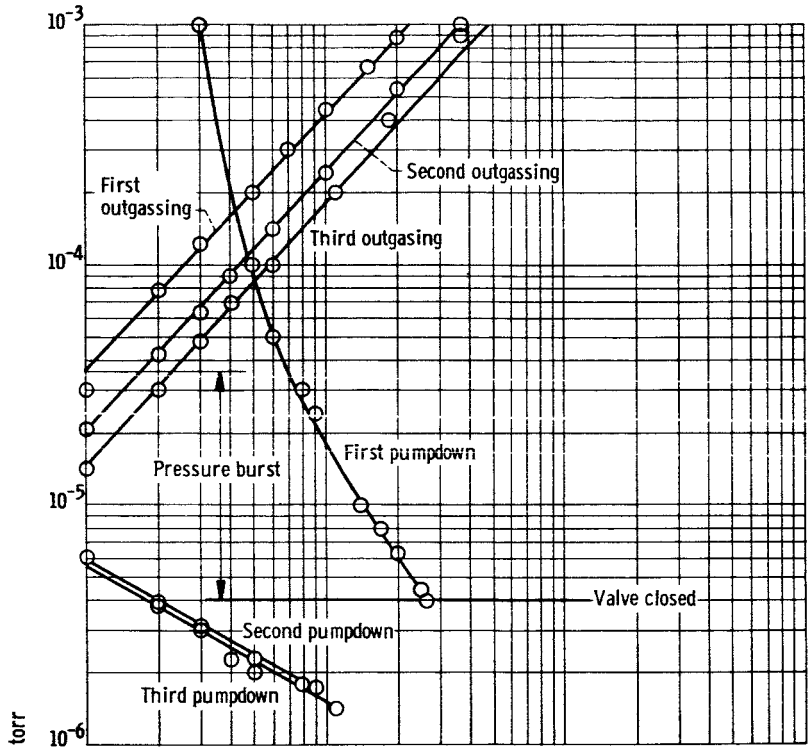

(a) Typical empty bell jar.

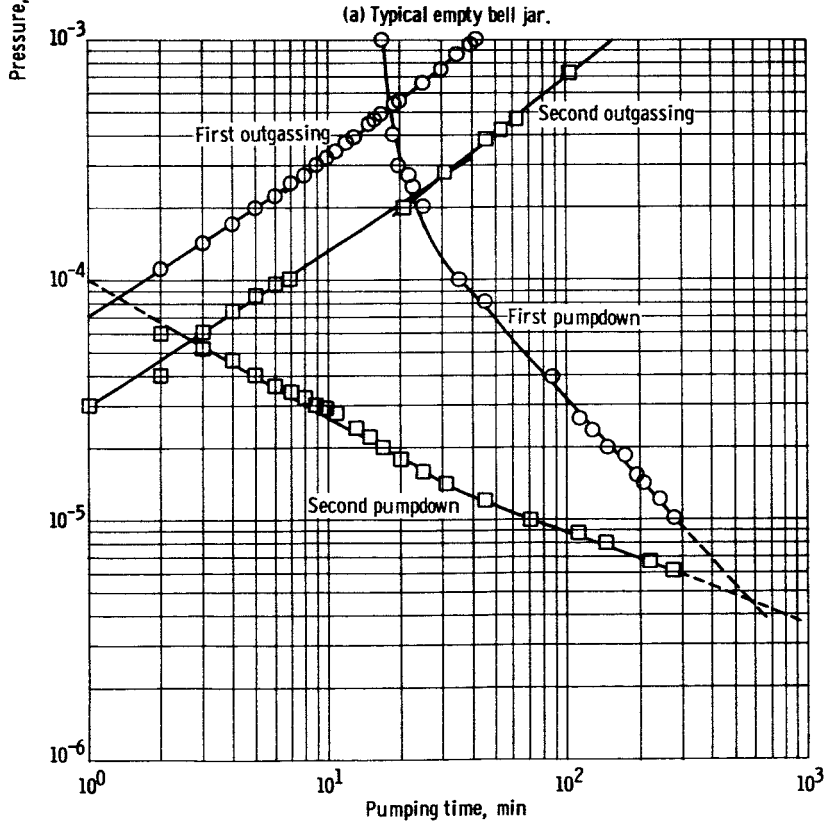

(b) Severely rusted carbon steel, specimen 1.

Figure 8. - Pressure-time history of bell jar.

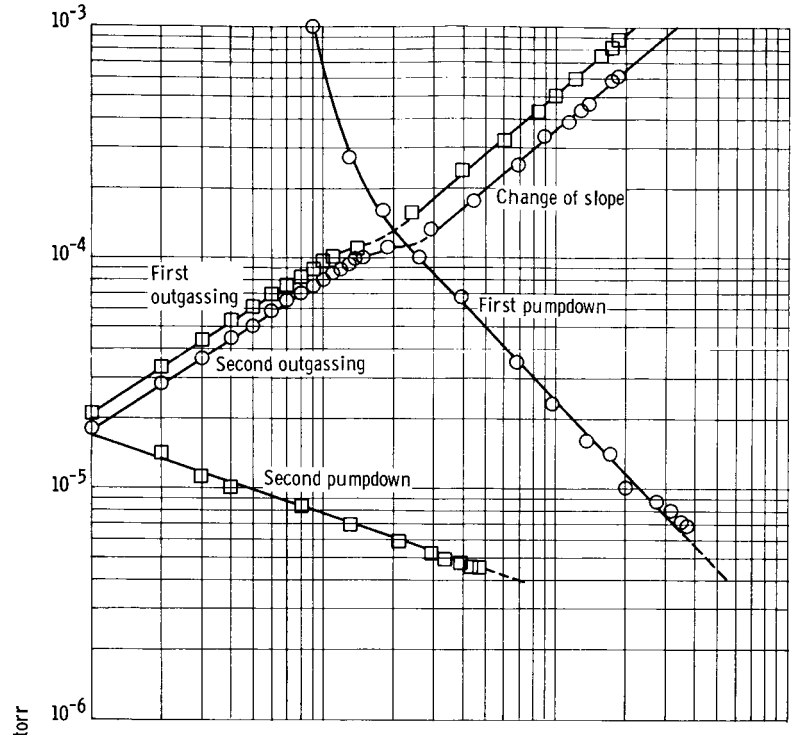

(c) Slightly rusted carbon steel, specimen 2. Change of slope was caused by calibration of instrument.

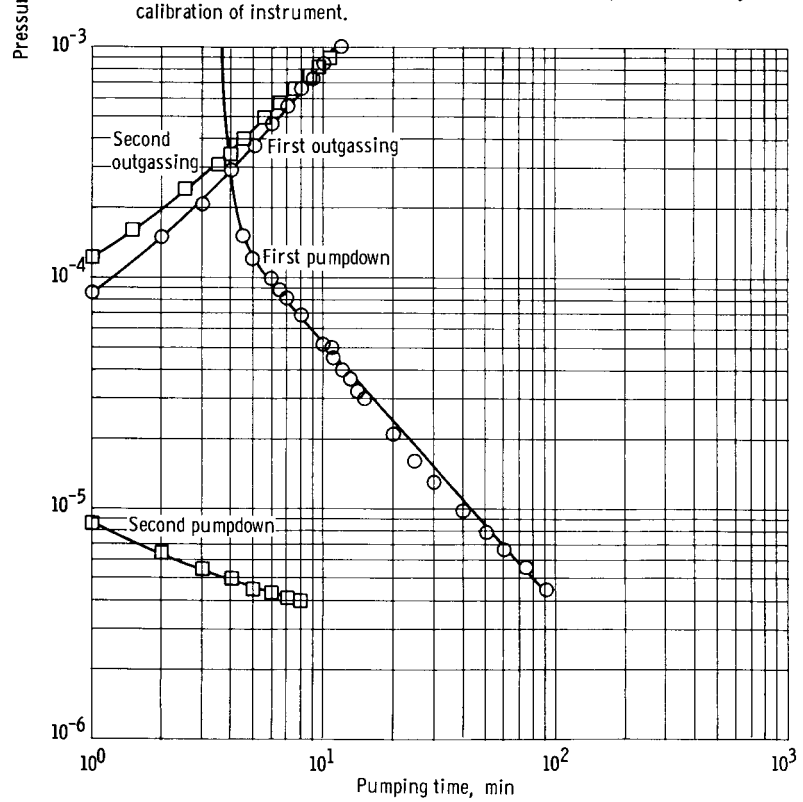

(d) Sandblasted carbon steel, specimen 3.

Figure 8. - Continued.

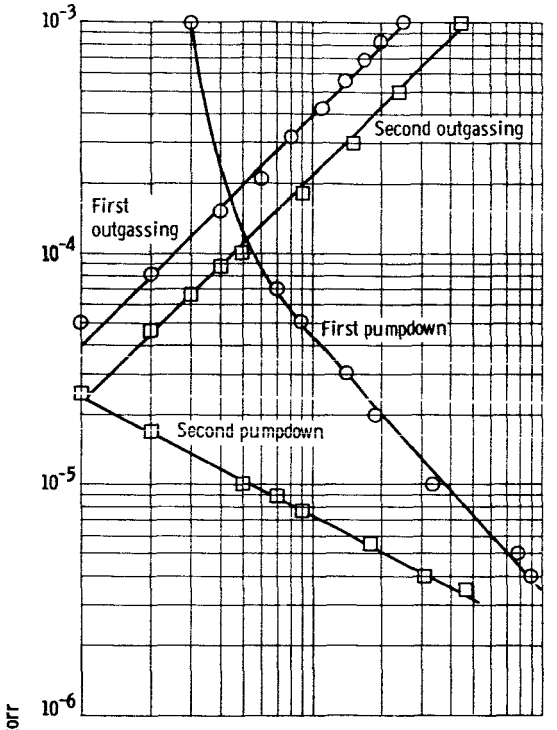

(e) Sandblasted and vapor degreased carbon steel, specimen 4.

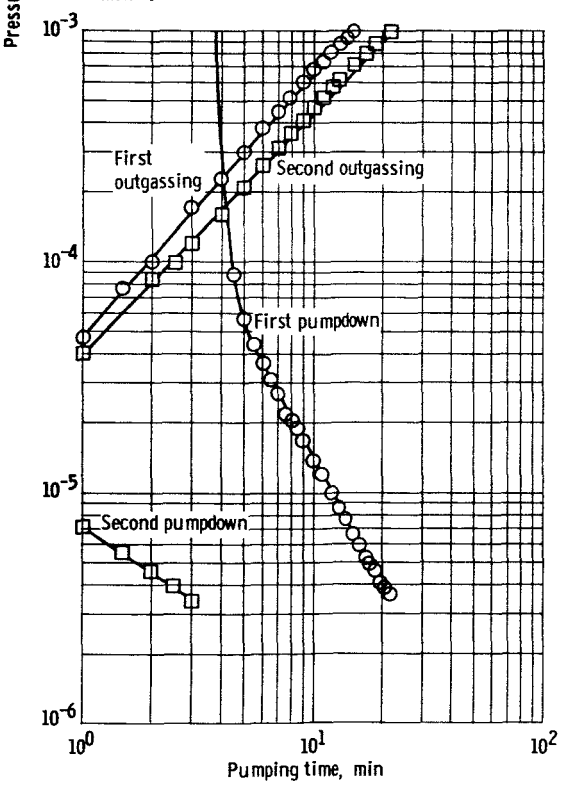

(f) AISI 304 stainless steel, specimen 5.

Figure 8. - Continued.

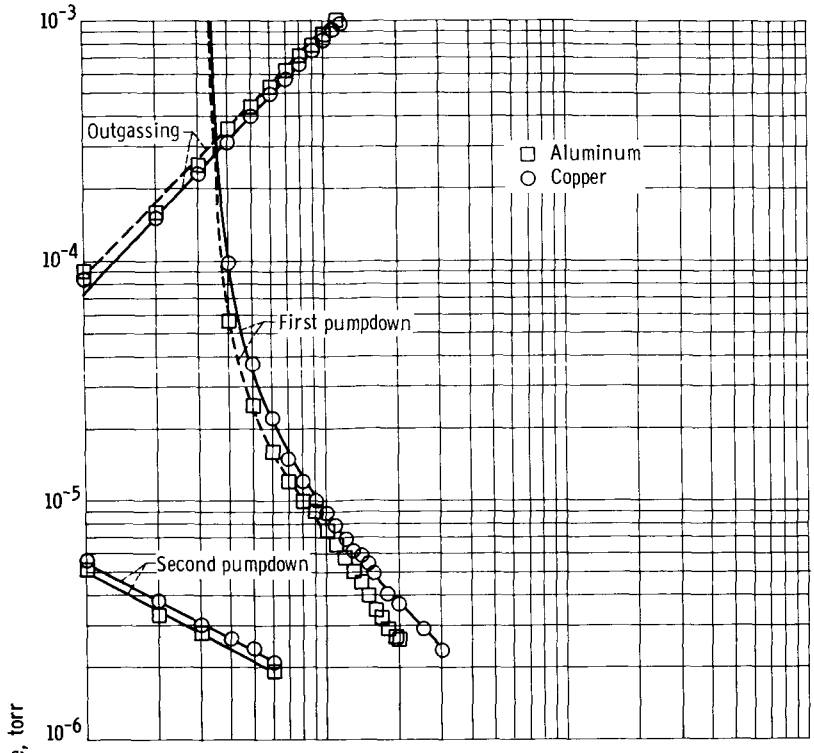

(g) Aluminum and copper, specimens 6 and 7.

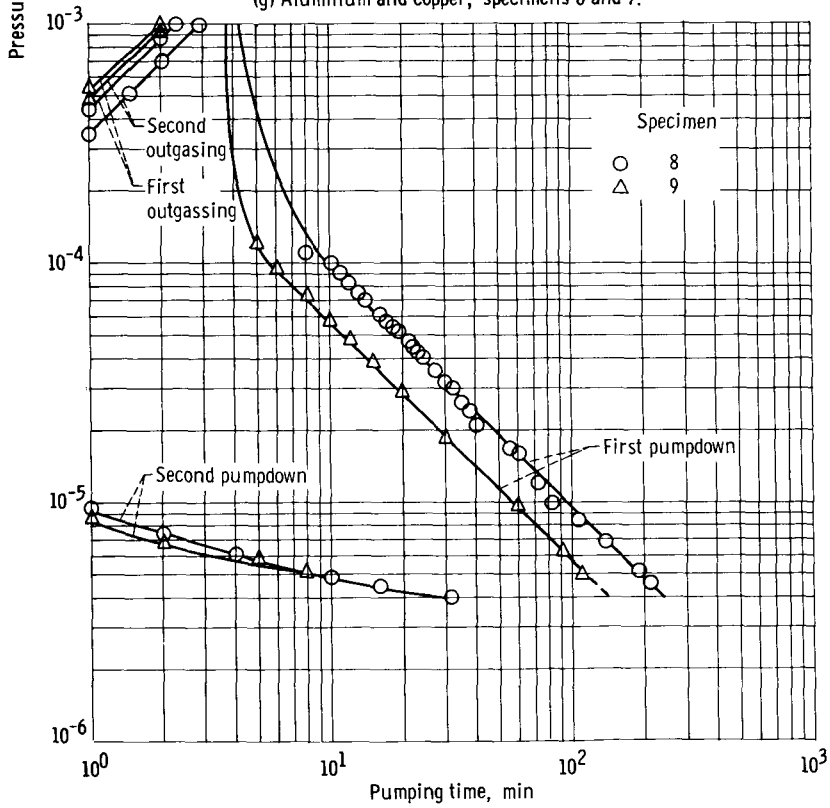

(h) Glyptal, specimens 8 and 9.

Figure 8. - Continued.

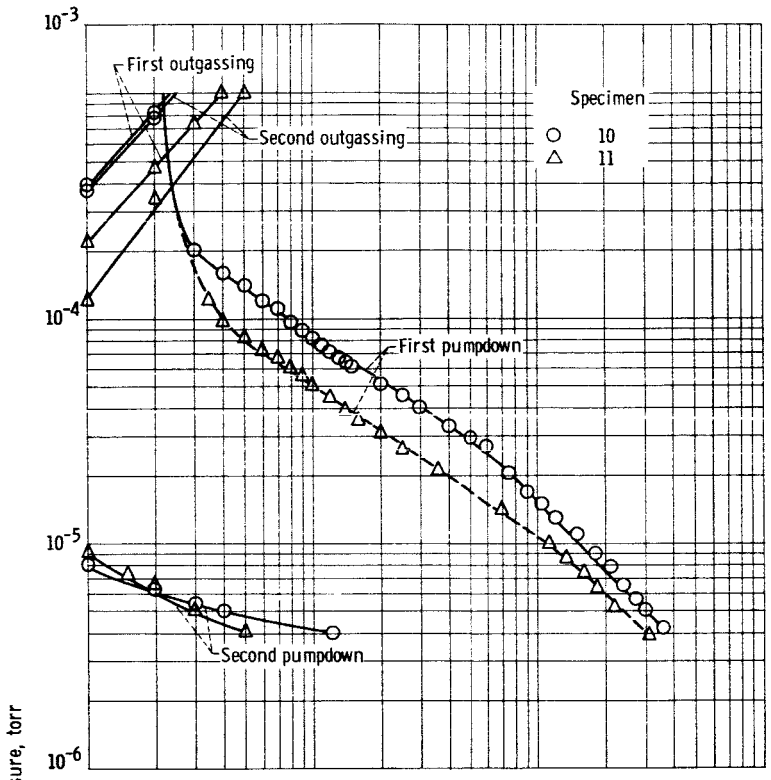

(i) Glyptal, specimens 10 and 11.

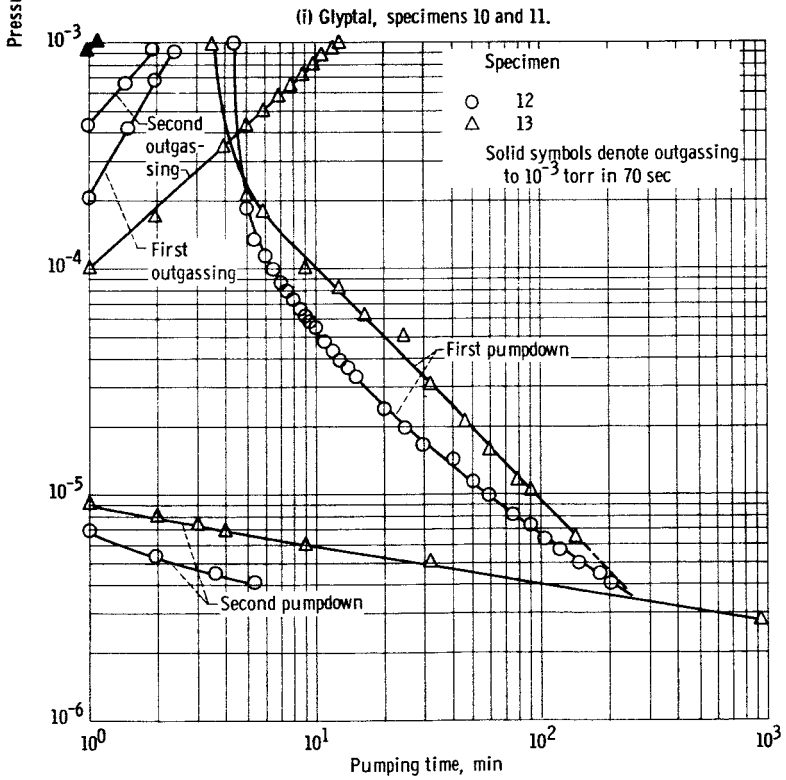

(j) Missile black, specimens 12 and 13.

Figure 8. - Continued.

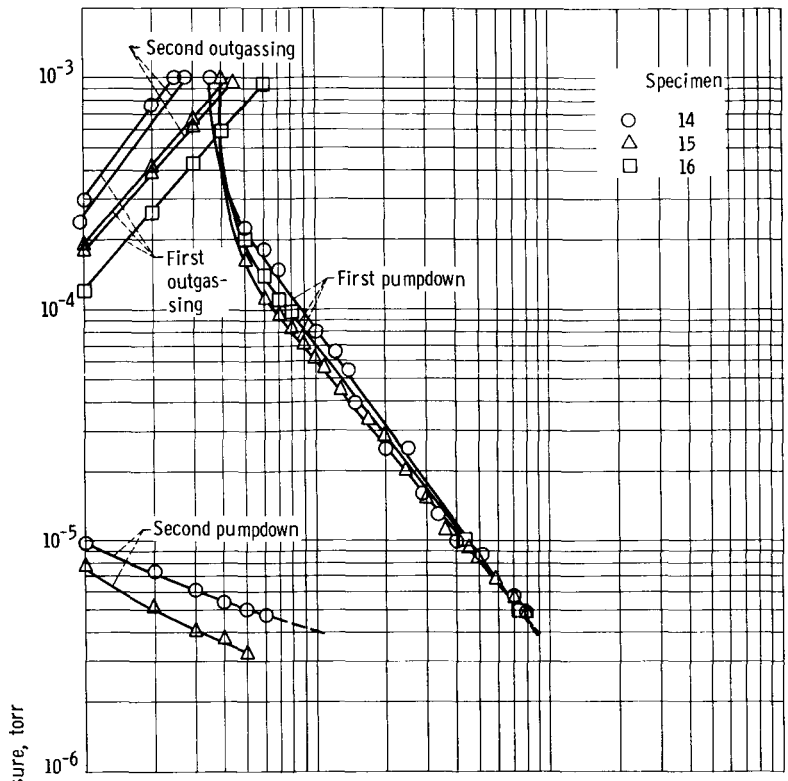

(k) Rust-Oleum clear, specimens 14, 15, and 16.

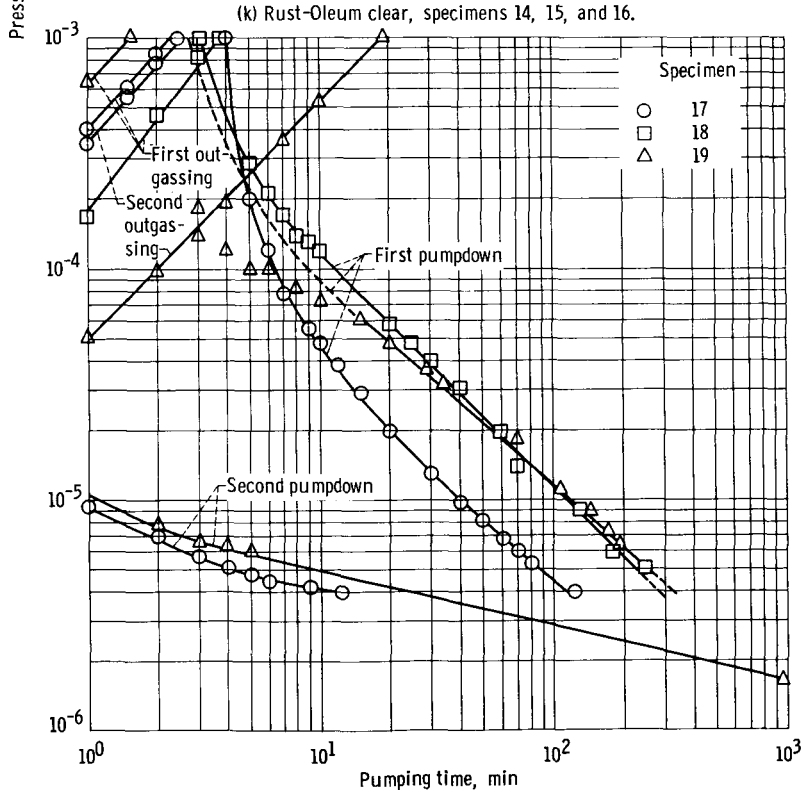

(l) Rust-Oleum red primer and green on red primer, specimens 17, 18, and 19.

Figure 8. - Continued.

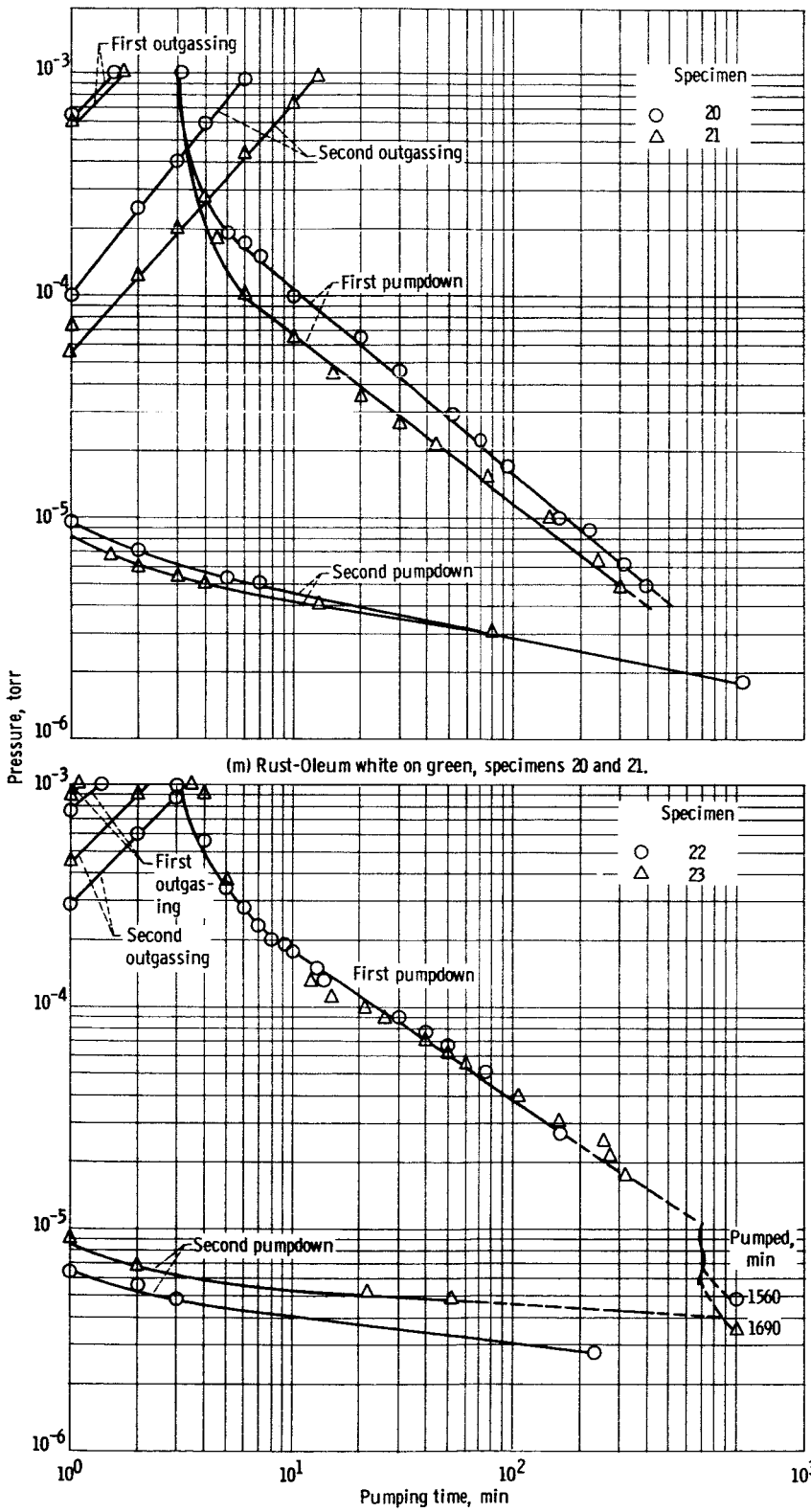

(m) Rust-Oleum white on green, specimens 20 and 21.

(n) Rust-Oleum gray and Rust-Oleum white, specimens 22 and 23.

Figure 8. - Continued.

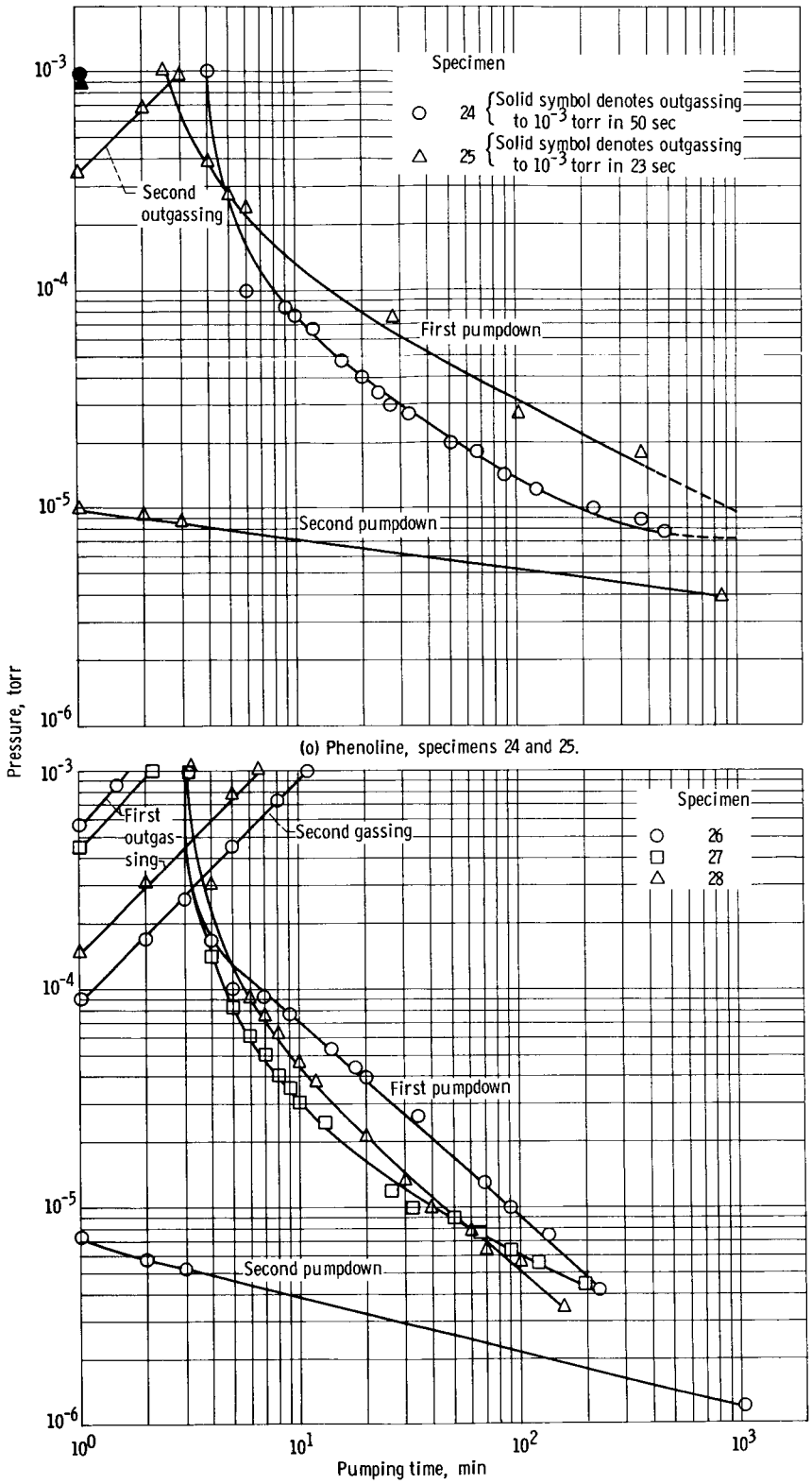

(o) Phenoline, specimens 24 and 25.

(p) Zinc chromate, white porcelain enamel, and white lacquer, specimens 26, 27, and 28.

Figure 8. - Continued.

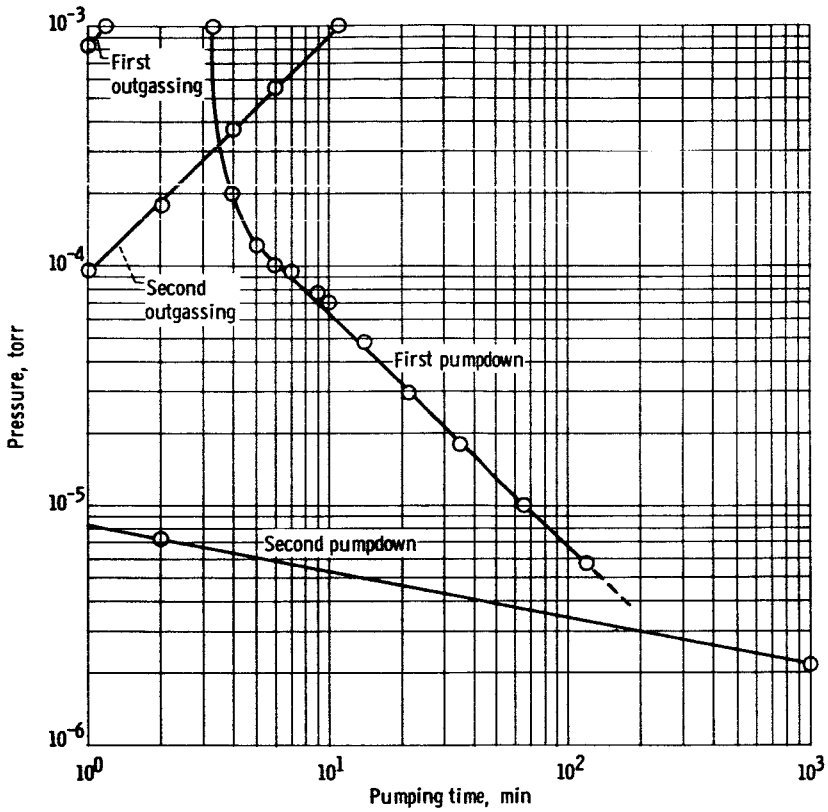

(q) Nylon, specimen 29.

Figure 8. - Concluded.

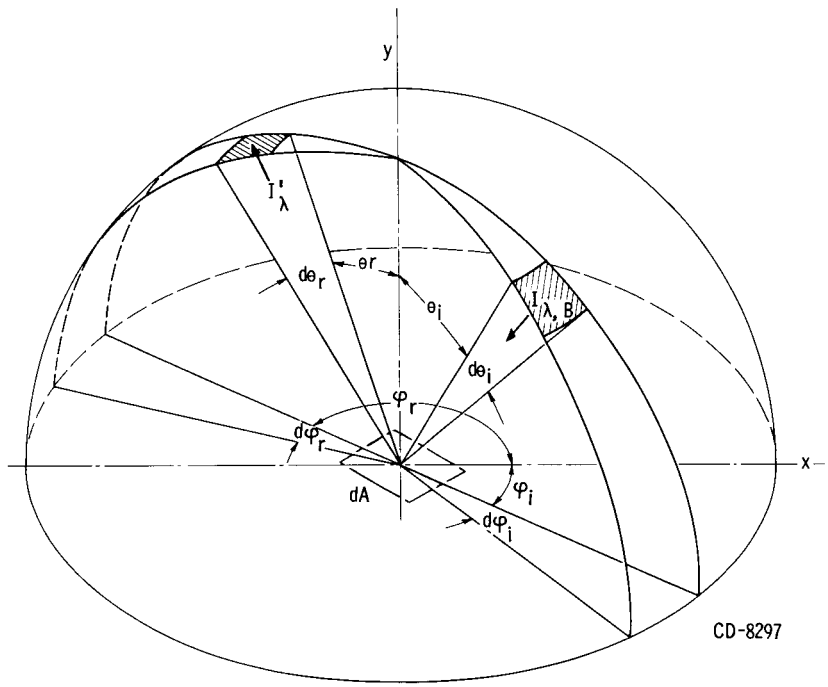

Figure 9. - Incident and reflected radiation at surface of sample.